Targeted Inhibition of lncRNA *Malat1* Alters the Tumor Immune Microenvironment in Preclinical Syngeneic Mouse Models of Triple-Negative Breast Cancer

Oluwatoyosi Adewunmi[1], Yichao Shen[2,3], Xiang H.-F. Zhang[3,4], and Jeffrey M. Rosen[3]

ABSTRACT

Long noncoding RNAs (lncRNA) play an important role in gene regulation in both normal tissues and cancer. Targeting lncRNAs is a promising therapeutic approach that has become feasible through the development of gapmer antisense oligonucleotides (ASO). Metastasis-associated lung adenocarcinoma transcript (*Malat1*) is an abundant lncRNA whose expression is upregulated in several cancers. Although *Malat1* increases the migratory and invasive properties of tumor cells, its role in the tumor microenvironment (TME) is still not well defined. We explored the connection between *Malat1* and the tumor immune microenvironment (TIME) using several immune-competent preclinical syngeneic *Tp53*-null triple-negative breast cancer (TNBC) mouse models that mimic the heterogeneity and immunosuppressive TME found in human breast cancer. Using a *Malat1* ASO, we were able to knockdown *Malat1* RNA expression resulting in a delay in primary tumor growth, decreased proliferation, and increased apoptosis. In addition, immunophenotyping of tumor-infiltrating lymphocytes revealed that *Malat1* inhibition altered the TIME, with a decrease in immunosuppressive tumor-associated macrophages (TAM) and myeloid-derived suppressor cells (MDSC) as well as an increase in cytotoxic $CD8^+$ T cells. *Malat1* depletion in tumor cells, TAMs, and MDSCs decreased immunosuppressive cytokine/chemokine secretion whereas *Malat1* inhibition in T cells increased inflammatory secretions and T-cell proliferation. Combination of a *Malat1* ASO with chemotherapy or immune checkpoint blockade (ICB) improved the treatment responses in a preclinical model. These studies highlight the immunostimulatory effects of *Malat1* inhibition in TNBC, the benefit of a *Malat1* ASO therapeutic, and its potential use in combination with chemotherapies and immunotherapies.

Introduction

Of increasing importance in the field of RNA biology is deciphering the function of long noncoding RNAs (lncRNA) and determining their utility as therapeutic targets. LncRNAs regulate a wide array of cellular functions, including nuclear organization, and transcriptional and posttranscriptional regulation, and are known to interact with miRNAs and effector proteins to alter gene expression (1–4). They also play a meaningful role in cancer progression and metastasis, and the expression of certain lncRNAs—for example, prostate cancer antigen 3—can be used as biomarkers for cancer diagnosis (5–7). LncRNAs are also known to regulate the immune response and can participate in immune cell activation and antigen presentation (8–10). The tumor microenvironment (TME) and the immune cells that make up the tumor immune microenvironment (TIME) are critical factors in cancer development and are potential targets for cancer treatment. Therefore, identifying and studying lncRNAs that can affect the TIME may lead to novel therapeutic strategies.

The highly invasive and aggressive nature of triple-negative breast cancer (TNBC; ref. 11) creates a challenge for effective treatment contributing to a lower progression-free survival (PFS) rate compared with other breast cancer subtypes (12). Immune checkpoint blockade (ICB) is now at the forefront of therapy and in combination with chemotherapy improves responses for patients with TNBC in both locally advanced and advanced stages of the disease (13, 14). The TNBC TIME is routinely comprised of a large number of tumor-associated macrophages (TAM) and myeloid-derived suppressor cells (MDSC) creating a highly immunosuppressive environment that promotes tumor-immune escape and invasion (15). This creates a challenge for therapies such as ICB and chemotherapy, and new approaches to help bolster immune infiltration and cytotoxicity are paramount for improving clinical responses.

Metastasis-associated lung adenocarcinoma transcript 1 (*Malat1*) is a lncRNA known to promote cell proliferation, invasion, and metastasis in numerous cancers (16–18). Breast cancers, including the TNBC subtype, have higher *Malat1* expression compared with adjacent normal tissue (19). Other studies have shown that patients with breast cancer with higher expression of *Malat1* have a lower recurrence-free survival as compared with those with lower or mid-levels of *Malat1* expression (20, 21). Knockdown of *Malat1* in a preclinical tumor model results in a decrease in the metastatic burden and increased differentiation (22). With respect to the TIME, *Malat1* has been shown to promote angiogenesis and immunosuppression in certain cancers (23, 24). However, the intrinsic effects of *Malat1* on immune cells and the TIME are still not well defined.

The primary goal of this study was to determine whether there could be a therapeutic benefit of *Malat1* inhibition in TNBC and to explore any role *Malat1* may have in regulating TIME dynamics. Targeting of *Malat1* was made possible with the use of gapmer

[1]Translational Biology and Molecular Medicine Program, Baylor College of Medicine, Houston, Texas. [2]Integrative Molecular and Biomedical Sciences Graduate Program, Baylor College of Medicine, Houston, Texas. [3]Department of Molecular and Cellular Biology, Baylor College of Medicine, Houston, Texas. [4]Lester and Sue Smith Breast Center, Dan L. Duncan Comprehensive Cancer Center, Baylor College of Medicine, Houston, Texas.

Corresponding Author: Jeffrey M. Rosen, Baylor College of Medicine, One Baylor Plaza, Houston, Texas 77030. E-mail: jrosen@bcm.edu

Cancer Immunol Res 2023;11:1462–79

doi: 10.1158/2326-6066.CIR-23-0045

antisense oligonucleotides (ASO), which have been successful in preclinical models for targeted knockdown of lncRNAs (22) and may provide a future therapeutic option. Advances in the development of second generation ASOs have improved the stability of ASOs with limited toxicity leading to clinical trials in several diseases, including cancer (25–27). To study the efficacy of targeted knockdown using an ASO in TNBC, we used the syngeneic *Tp53*-null preclinical mouse models that have been extensively characterized both genetically and with respect to their TIME (28, 29). In these models, knockdown of *Malat1* RNA expression *in vivo* delayed primary tumor growth and significantly decreased tumor volume, with decreased tumor cell proliferation and increased apoptosis. Furthermore, analysis of tumor-infiltrating lymphocytes (TIL) and *in vitro* coculture assays of myeloid cells and T cells revealed that *Malat1* inhibition shifted the TIME to a more immunostimulatory state.

Materials and Methods

Cell culture

All *Tp53*-null tumor-derived cell lines were created in the Rosen Laboratory as previously reported (30) and are tested for *Mycoplasma* periodically using the Universal *Mycoplasma* Detection Kit (ATCC). *Mycoplasma* testing for these cell lines was last performed in April, 2019. T11 and T12 cells were cultured in DMEM/F12 with no phenol red (GeneDEPOT, CM018–300) and supplemented with 10% heat-inactivated FBS (GeneDEPOT, F0900–050), 5 μg/mL insulin (Sigma, I-5500), 10 ng/mL EGF (Sigma, SRP3196), 1 μg/mL hydrocortisone (Sigma, H0888), and 100 U/mL antibiotic–antimycotic (Thermo Fisher Scientific, 15240062). 2208 L cells were cultured in DMEM media (GenDEPOT, CM002–050) supplemented with 10% heat-inactivated FBS and 100 U/mL antibiotic–antimycotic. Cell lines were incubated in humidified incubator at 37°C with 5% CO_2. When cells from frozen stock are thawed and plated new frozen stocks are created without further passages. Cells used for experiments are used within 5 passages of being thawed from frozen stocks. GFP-labeled T12 cells were generated by lentiviral transduction of GFP reporter plasmids as described previously (31). Briefly, GFP reporter plasmids were transfected together with psPAX2 and pMD2.G packaging plasmids into HEK293T cells using X-tremeGENE HP DNA transfection reagent (Sigma, 6366244001). 48 hours later, the viral supernatant was harvested and filtered by 0.45-μm-filter (VWR International, 76479–020). T12 cells were transduced with lentivirus and 8 μg/mL polybrene (Sigma, TR-1003). Two days later, GFP-positive cells were sorted using a SONY MA900 sorter to generate a reporter cell line.

ASO transfection

All ASOs used for this study were generously supplied by Ionis and Flamingo Pharmaceuticals. These compounds are 3–10–3 cEt gapmers and the sequence of the ASO used are shown in Supplementary Table S1. To determine the concentration required for ≥50% *Malat1* depletion, dosing experiments were performed in T11 and 2208 L cell lines and 250 and 750 nmol/L of ASO, respectively, were used for all subsequent tumor cell line–specific experiments (Supplementary Fig. S1A and S1B). In Claudin-low tumor cell lines (T11 and T12) an ASO transfection reagent was needed to achieve *Malat1* knockdown.

T12 and T11 tumor cells were seeded in 6-well plates at a cell density between a total of 2.0×10^5 and 2.5×10^5 cells per well 24 hours before transfection. A transfection cocktail consisting of 250 μL Opti-MEM serum-free media (Thermo Fisher Scientific, 31985070), 15 μL oligo transfection reagent (Mirus Bio, MIR 2160), and 250 nmol/L of either *Malat1* ASO or a nontargeted Scramble ASO per well was incubated for 20 minutes at room temperature and added drop-wise to cells. Cells were harvested for analysis by RT-qPCR 48 hours after transfection. 2208 L tumor cells were treated with 750 nmol/L of ASO in cell culture media without oligo transfection reagent.

RT-qPCR

RNA was harvested using either an RNeasy mini-isolation kit (Qiagen, 74104) or TRizol (Thermo Fisher Scientific, 15596018) and 1 μg of RNA was used to make cDNA using a High-Capacity cDNA Reverse Transcription Kit (Thermo Fisher Scientific, 4368814). 5 μg of cDNA was added to a cDNA cocktail containing 1x amfisure qGreen Q-PCR Master Mix (GenDEPOT, Q5602–005) and *Malat1*-specific reverse and forward primers (Forward: TCTTCTATTCTTGGGCTTCCTACT, Reverse: AAGCATCTTTAGAAGACAGAAAAG). *Neat1* RNA expression (Forward: TGTTAAAGGCGCTTTGGAAG, Reverse: GCGGGGCTAAGTATAAAGGAG) was quantified as well. *Malat1* and *Neat1* expressions were normalized to *Gapdh* (Forward: CTGGAGAAACCTGCCAAGTAT, Reverse: GAGTTGCTGTTGAAGTCGCAG) expression in cells and the relative RNA expression was calculated using the $\Delta\Delta C_t$ relative fold change method. All RT-qPCR experiments were performed on the StepOnePlus Real-Time PCR System (Thermo Fisher Scientific, 4376600).

Animal studies

All animal experiments were performed in the Baylor College of Medicine animal facility with 12-hour day or night cycles. Animal experiments were performed in accordance with the Baylor College of Medicine Animal Care and Use Committee (IACUC)-approved protocol (AN-504). Studies complied with all ethical regulations regarding animal research.

Single-agent ASO treatment

Tp53-null tumor pieces from either the Claudin-low models (T11 and T12) or the luminal-like model 2208 L were kept frozen in an established tumor bank in the Rosen Laboratory. For treatment experiments, frozen tumor pieces were thawed and implanted into the mammary fat pad of a 7- to 10-week-old donor wild-type (WT) BALB/c mouse (Envigo Laboratories). The tumor was harvested when it reached approximately 500 mm^3 and implanted into the 4th mammary fat pad of 7- to 10-week-old WT BALB/c mice. Once tumors were palpable and ≤50 mm^3 in volume, mice were randomized into a *Malat1* ASO treatment group and a nontargeted Scramble ASO control group. For randomization, mice were weighed and had their tumor size measured using digital calipers. Mice were then assigned a number and numbers were randomly placed in two groups using Excel. Mice implanted with Claudin-low tumors received a 25 mg/kg subcutaneous injection of *Malat1* ASO or a nontargeted Scramble ASO daily and mice implanted with the 2208 L tumors received a 50 mg/kg subcutaneous injection. The appropriate dosage was determined by a short 5-day ASO treatment of tumors to confirm *Malat1* knockdown in the tumors. Mice were weighed and had their tumors measured and recorded every 2 to 3 days. Mice were sacrificed after 14 days for short treatment studies or once the tumor reached an approximate volume of 1,500 mm^3 for survival studies. Tumor volume was calculated using length × width × width/2. Tumors were harvested and center sections were fixed with either 4% paraformaldehyde (Sigma, P6148) or 10% formalin (Thermo Fisher Scientific, 22–050–105), small sections were cryopreserved for RNA and protein extraction, and the remaining tumor was digested with 1 mg/mL Collagenase Type 1 (Sigma-Aldrich, 11088793001) for the isolation of TILs.

ASO treatment in T cell–deficient mice

To assess the effects of *Malat1* ASO or a nontargeted Scramble ASO in T cell–deficient mice, 6- to 7-week-old nude mice (Hsd: Athymic Nude-Foxn1nu; Envigo Laboratories, 069) were implanted with 2208 L tumors and treated with 50 mg/kg of single-agent ASO once tumors were palpable. In addition, $CD8^+$ T-cell depletion treatment studies were performed using, 6- to 7-week-old WT BALB/c mice implanted with 2208 L tumors and treated with blocking antibody (BioXcell; clone 2.43, BE0061) once every 4 days. Once tumors were palpable, mice were randomized into four groups and treated as follows: 250 μg anti-CD8α (BioXcell; clone 2.43, BE0061) + 50 mg/kg Scramble ASO, 250 μg anti-CD8α + 50 mg/kg *Malat1* ASO, 250 μg IgG2b (BioXcell; clone LTF-2, BE0090) + 50 mg/kg Scramble ASO, and 250 μg IgG2b + 50 mg/kg *Malat1* ASO. Mice were sacrificed after 14 days of treatment.

Chemotherapy/checkpoint and ASO combination treatment

For separate combination studies, 2208 L tumor pieces were implanted into WT BALB/c mice and 25 mg/kg of Carboplatin (Sigma-Aldrich, C2538) was injected intraperitoneally weekly in combination with daily injection of either *Malat1* ASO or Scramble ASO control. Combination studies using 2208 L primary tumors treated with anti-PD1 checkpoint inhibitor were also performed and 10 mg/kg of anti-PD1 antibody (Bio X Cell Clone: RMP1–14, BE0146) was injected intraperitoneally once every 72 hours in combination with daily ASO injection. A small cohort of mice was treated with an IgG2b control (Bio X Cell Clone: MPC-11, BE0086). Mice were sacrificed after 5 or 14 days for short treatment studies or once the tumors reached an approximate volume of 1,500 mm^3 for survival studies.

Isolation of TILs

Tumors were minced using a McIlwain tissue chopper and digested in digestion medium comprising 1 mg/mL Collagenase Type 1 and 1 μg/mL DNase (Sigma-Aldrich, 11284932001) in DMEM/F12 media with no additives for 2 hours at 37°C on a rocker. Digestions were then spun down at 1,500 rpm and the supernatant was discarded. Pellets were resuspended in PBS (Thermo Fisher Scientific, BP3994 or GenDEPOT, CA008–050) and underwent 3 short centrifugations, collecting the supernatant into a separate tube after each spin. The collected supernatant was then spun down and the pellet was resuspended in 1x RBC lysis buffer (BioLegend, 420301) and incubated in ice for 3 minutes. PBS was added after incubation to stop the reaction and spun down at 1,500 rpm. The pellet was resuspended in staining buffer (PBS with 2% FBS) and passed through a 40-μm mesh filter (VWR 352340). Live cells were counted with trypan blue (Bio-Rad, 1450021) using a Bio-Rad TC20 Cell Counter and 1 million cells were plated per panel in 96-well nontreated tissue culture plate (Thermo Fisher Scientific 50202148) for flow cytometry.

Histology

Fixed tumor sections were paraffin-embedded and 5-μm tissue sections were used for IHC staining.

IHC staining

Paraffin-embedded tissue sections were washed and permeabilized using xylene (Thermo Fisher Scientific, 22050283) and 100%, 95%, 80%, and 75% ethanol. Sections underwent antigen retrieval using a Tris-EDTA antigen retrieval buffer (10 mmol/L Trisbase, 1 mmol/L EDTA) for 20 minutes and were then rinsed three times in deionized (DI) water and PBS for 5 minutes each. Sections were then blocked in a hydrogen peroxide solution (Thermo Fisher Scientific, H323–500) for 10 minutes and further blocked for 1 hour in a blocking buffer consisting of 3% BSA (Thermo Fisher Scientific, NC1235497), 2% Goat serum (Sigma-Aldrich, G9023), and 0.01% Tween (Millipore Sigma, 11332465001) in PBS for rabbit antibodies or blocked using the M.O.M blocking buffer (Vector Laboratories, BMK-2202) for mouse or rat antibodies. After blocking, sections were incubated with primary antibodies [Phospho-histone 3 (1:1,000; Cell Signaling Technology, 9701S)], Cleaved Caspase 3 (1:1,000; Cell Signaling Technology, 9661S), CD8α (1:750; Thermo Fisher Scientific, 14–0081–82), Foxp3 (1:500; Cell Signaling Technology, 12653T), F4/80 (1:500; Cell Signaling Technology, 70076S), or S100a8 (1:5,000; Thermo Fisher Scientific, MAB3059) at 4°C overnight and the next day washed three times with PBS for 10 minutes each and incubated with horseradish peroxidase (HRP)–conjugated secondary antibody for rat (Vector Laboratories, PI-9400–1) or rabbit (Vector Laboratories, PI-1000–1) at 1:1,000 concentration for 1 hour at room temperature. Sections were then incubated with VECTASTAIN Elite ABC HRP Reagent (Vector Laboratories, PK7100) for 30 minutes, washed with PBS three times and treated with ImmPACT DAB peroxidase substrate (Vector Laboratories, sk-4105) before being rinsed with DI water. Sections were then counterstained with hematoxylin (Poly Scientific, S212A) and once dry, mounted in Poly-Mount Xylene (Poly Scientific, 24176–120). 3 to 5 microscopic images were taken for each slide using the Olympus BX40 light microscope and Magnafire camera at a 20× objective. Positive staining was quantified using ImageJ (ImageJ, RRID:SCR_003070; ref. 32). Briefly, images were converted to 8-bit and threshold was adjusted to remove background from each image. The percentage of the positive area of up to 3 representative images from each tissue section was calculated and 5 to 8 tissue sections were used for each treatment group.

Flow cytometry

TILs

A total of 1.0×10^6 TILs were stained with Live/Dead Fixable Yellow (Thermo Fisher Scientific L34968) at a 1:1,000 concentration for 30 minutes on ice, rinsed with staining buffer and then blocked with CD16/32 FCR blocker at a 1:100 concentration (BioLegend, 101319) for 30 minutes on ice. Cells were then stained with antibodies specific for cell surface markers at a previously validated concentration for 30 minutes on ice. Two panels of antibodies were used to immunophenotype TILs and they were as follows; Panel 1–Cd11c Pacific Blue (BioLegend, 117322), MHCII BV711 (BioLegend, 107643), CD86 FITC (BioLegend, 105006), CD11b PerCP CY 5.5 (BioLegend, 101227), Ly-6C PeCy7 (BioLegend, 128017), F4/80 APC (BioLegend, 123115), CD45 Alexa Fluor 700 (BioLegend, 103128), and Ly6-G APC/Fire 750 (BioLegend, 127651). Panel 2–CD45 Pacific Blue (BioLegend, 103126), CD3ε PerCP Cy 5.5 (BioLegend, 100218), CD45R (B220) PE-CY7 (BioLegend, 103221), CD8α Alexa Fluor 700 (BioLegend, 100730), CD49b (pan-NK cells) PE/Dazzle 594 (BioLegend, 108924), and CD4 APC/Fire 750 (BioLegend, 100460). After surface staining, cells were rinsed with PBS and fixed overnight at 4°C using a Foxp3/Transcription Factor Staining Buffer Set (Thermo Fisher Scientific, 00–5523–00). After fixation cells were blocked in permeabilization buffer (Thermo Fisher Scientific, 00–5523–00) with 2% rat serum (Sigma-Aldrich, R9759) for 30 minutes at room temperature and then stained with antibodies specific for intracellular markers. Panel 1 contained antibodies specific for Arginase PE (Thermo Fisher Scientific, 12–3697–82), CD206 PE/Dazzle 594 (BioLegend, 141732) for T12 TILs and Panel 2 antibodies specific for contained Ifnγ FITC (BioLegend, 505806), Foxp3 PE (BioLegend, 126403), and Granzyme B APC (BioLegend, 372203). After staining, cells were washed twice

with permeabilization buffer, resuspended in PBS and data were collected using the Attune NxT flow cytometer. Flow samples were properly compensated and analyzed using FlowJo v10 software (FlowJo, RRID:SCR_008520).

Peripheral blood mononuclear cells

To validate depletion of CD8α$^+$ cells, blood was collected retro-orbitally using capillary tubes (Thermo Fisher Scientific, 22- 362566) and red blood cells were lysed for 30 minutes using red lysis buffer (Thermo Fisher Scientific, 00–4333–57). Cells were blocked for 30 minutes using anti CD16/32 FCR blocker and then stained with CD3ε PerCP Cy 5.5 (BioLegend, 100218), CD8α Alexa Fluor 700 (BioLegend, 100730), and CD4 APC/Fire 750 (BioLegend, 100460) antibodies for 30 minutes on ice. After staining, cells were resuspended in PBS (GenDEPOT, CA008–050) containing NucBlue Live Ready-Probes (Thermo Fisher Scientific, R37605) and data were collected using the Attune NxT flow cytometer.

***In vitro* myeloid cells**

Myeloid cells collected from either T12 or 2208 L primary tumors were stained with Live/Dead Fixable Yellow (Thermo Fisher Scientific L34968) at a 1:1,000 concentration for 30 minutes on ice, rinsed with staining buffer, and then blocked with CD16/32 FCR blocker at a 1:100 concentration (BioLegend, 101319) for 30 minutes on ice. Cells were then stained with cell surface markers for 30 minutes on ice. The surface markers analyzed were: MHCII BV711 (BioLegend, 107643), CD86 Alexa Fluor 700(BioLegend, 105024), CD11b PerCP CY 5.5 (BioLegend, 101227), Ly-6C PeCy7 (BioLegend, 128017), F4/80 APC (BioLegend, 123115), and Ly6-G APC/Fire 750 (BioLegend, 127651). Data were collected using the Attune NxT flow cytometer.

***In vitro* T cells**

T cells collected from the spleen of WT BALB/c mice were stained with Live/Dead Fixable Yellow (Thermo Fisher Scientific L34968) at a 1:1,000 concentration for 30 minutes on ice, rinsed with staining buffer, and then blocked with CD16/32 FCR blocker at a 1:100 concentration (BioLegend, 101319) for 10 minutes on ice. Cells were then stained with antibodies specific for cell surface markers for 30 minutes on ice. The surface markers analyzed were: CD3ε PerCP Cy 5.5 (BioLegend, 100218), CD8α Alexa Fluor 700 (BioLegend, 100730), and CD4 APC/Fire 750 (BioLegend, 100460) After surface staining, cells were rinsed with PBS and fixed for 20 minutes at room temperature using a Foxp3/Transcription Factor Staining Buffer Set (Thermo Fisher Scientific, 00–5523–00). After fixation, cells were stained with antibodies specific for intracellular markers: Granzyme B APC (BioLegend, 372203) and Perforin PE (BioLegend, 154405). Data were collected using the Attune NxT flow cytometer.

***In vitro* T-cell proliferation assay**

To assess changes to T-cell function, proliferation assays were performed on naïve splenocytes isolated from WT BALB/c mice. Red blood cells were lysed using 1X RBC lysis buffer and CD3$^+$ T cells were enriched using negative selection of biotinylated antibodies B220, CD11b, and Gr-1 (#559971, BD Pharmingen, RRID:AB_10053179), magnetically sorted using the EasySep Mouse Biotin Positive Selection Kit (#18559, Stemcell), and stained with carboxyfluorescein diacetate succinimidyl ester (CFSE; Thermo Fisher Scientific, C34570). First, cells were washed with PBS and the pellet was resuspended in a CFSE labeling solution consisting of 1.5 μmol/L CFSE in 0.1% FBS and incubated at room temperature for 10 minutes. Equal volume of warmed FBS was added to solution and cells were further incubated at 37°C for 10 minutes. Cells were centrifuged at 1,500 rpm and washed with PBS + 2% FBS. Cells were then counted using trypan blue and plated in 24-well culture plates in T-cell media consisting of 10% FBS, 2 mmol/L Glutamax (Thermo Fisher Scientific 35050061), 5 mmol/L sodium pyruvate (Thermo Fisher Scientific 11360070), 5 mmol/L NEAA (Thermo Fisher Scientific 11–140–050), 55 μmol/L BME (Thermo Fisher Scientific 21985023) in RPMI media (GenDEPOT CM058–050). 10 ng/mL IL2 (BioLegend, 575404) was added to the culture every 2 to 3 days. To determine the concentration required for *Malat1* depletion, dosing experiments were performed on stimulated T cells. Cells were either left unstimulated or stimulated at a 1:1 ratio using anti-CD3/anti-CD28–coated Dynabeads (Thermo Fisher Scientific, 11456D) and after 48 hours of incubation, 500 nmol/L of either *Malat1* ASO or Scramble ASO was added to the culture medium and replenished every 48 hours. Two separate *Malat1*-targeting ASOs and two nontargeted Scramble ASO were tested. Cells were collected on days 3 and 5 and quantified using flow cytometry. Furthermore, intracellular staining of T-cell activation markers, Granzyme B APC (BioLegend, 372203) and Perforin (BioLegend, 154405) was performed. Data were collected using Attune NxT flow cytometer and analyzed using FlowJo v10 software.

***In vitro* T-cell suppression assay**

To assess whether myeloid cell function was altered with *Malat1* depletion, TAMs and MDSCs were isolated from tumor-bearing mice and cocultured with activated CD3$^+$ T cells isolated from naïve splenocytes of BALB/c mice. T12 and 2208 L tumors were digested as previously described (see *Isolation of TILs*) and either TAMs or MDSCs were isolated from the harvested TILs using the EasySep F4/80$^+$ positive selection kit (STEMCELL, 100–0659) and the EasySep CD11b GR1$^+$ isolation kit (STEMCELL Technologies, 19867), respectively. Isolated myeloid cells were plated in 24-well culture plates at a 125k cell density in T-cell media supplemented with 20% conditioned media collected from the supernatant of either T12 or 2208 L tumor cells. Myeloid cells without T cells were cultured in 10% FBS, 55 μmol/L BME, and 100 U/mL antibiotic–antimycotic in RPMI media supplemented with 20% conditioned media. To determine the ASO concentration required for *Malat1* depletion in myeloid cells, dosing experiments were performed in TAMs isolated from T12 primary tumors. To assess T-cell suppression, stimulated T cells stained with CFSE were added to myeloid cell cultures at myeloid cell:T-cell ratios of 0:5:1 and 1:1. Cocultures were treated with 250 nmol/L of ASO and incubated for 72 hours. T cells were collected, magnetically separated from the activation beads and CFSE dilution was analyzed using flow cytometry. Intracellular staining of the T-cell activation markers Granzyme B APC and Perforin PE was performed and quantified. Two separate *Malat1*-targeting ASOs and two non-targeted Scramble ASO were tested. Data were collected using Attune NxT Flow Cytometer and analyzed using FlowJo v10.

T-cell suppression was also assessed using GFP-targeted T cells isolated from the splenocytes of Just EGFP Death–Inducing (JEDI) mice (C57bL/6), cultured with a GFP-labeled T12 tumor-derived cell line, and with TAMs or MDSCs isolated from a T12 primary tumor at a 1:1:1 or 5:5:1 T-cell:TAM/MDSC:tumor cell ratio. JEDI mice carry a GFP-specific T-cell receptor transgene. JEDI mice for this study were kindly gifted by Dr. Brian Brown (Icahn School of Medicine at Mt. Sinai). Cocultures were treated with 250 nmol/L of ASO and incubated in the Incucyte S3 Live-Cell Analysis instrument where fluorescence and phase images were taken every 2 hours for approximately 72 hours. Myeloid cells were cultured with tumor cells without T cells as a control. After approximately 72 hours, T cells were collected

from wells and stained with antibodies specific for surface markers—CD3ε PerCP Cy 5.5, CD8α Alexa Fluor 700, and CD4 APC/Fire—and intracellular T-cell activation markers—Granzyme B APC and Perforin PE. Residual tumor cells were collected from the wells and stained with cell death marker Annexin V (BioLegend, 64093). Data were collected using Attune NxT flow cytometer and analyzed using FlowJo v10 software.

In vitro T-cell function assay

To carry out T-cell functional studies, $CD3^+$ T cells were isolated as previously described (see *In vitro* T-cell proliferation assay) from the spleen of JEDI mice and activated at a 1:1 ratio with anti-CD3/anti-CD28–coated Dynabeads for 72 hours in T-cell media. Activated T cells were magnetically separated from the beads and cultured with GFP-labeled T12 tumor cells at various effector:target (E:T) ratios (1:1, 5:1, and 10:1). Cocultures were treated with 500 nmol/L of ASO and incubated in the Incucyte S3 Live-Cell Analysis Instrument where fluorescence and phase images were taken every 2 hours for 24 to 48 hours at a 4× objective. After 48 hours, T cells were collected from wells and stained with antibodies specific for surface markers—CD3ε PerCP Cy 5.5 (BioLegend, 100218), CD8α Alexa Fluor 700 (BioLegend, 100730), and CD4 APC/Fire 750 (BioLegend, 100460)—and intracellular T-cell activation markers—Granzyme B APC (BioLegend, 372203) and Perforin PE (BioLegend, 154405). Residual tumor cells also were collected from the well and stained with the cell death marker Annexin V (BioLegend, 64093). Changes in GFP signal was calculated by dividing the total green object–integrated intensity (GCU × μm^2/image) at the endpoint by the starting green object–integrated intensity (GCU × μm^2/image). GFP signal was recorded using Incucyte S3. Data were collected using Attune NxT flow cytometer and analyzed using FlowJo v10 software. Supernatants from the different experimental groups were also collected for cytokine profiling.

Cytokine profiling

To determine tumor intrinsic changes to the cytokine profile after *Malat1* knockdown, cell supernatant, cell lysate, and tissue homogenate were assayed using the Mouse Cytokine/Chemokine 31-Plex Discovery Assay (Eve Technologies Corp.). Tissue homogenates were prepared using a tissue protein extraction reagent (Thermo Fisher Scientific, 78510) and cells were lysed using an NP-40 lysis buffer (50 mmol/L Tris-Base, 150 mmol/L NaCl, 1.0% NP-40, and cOmplete, EDTA-free Protease Inhibitor Cocktail; Sigma-Aldrich, 11873580001). Heat maps of differentially expressed cytokines or chemokines were generated using Morpheus (https://software.broadinstitute.org/morpheus). Supernatant of cocultures with tumor cells, JEDI T cells, and myeloid cells were assayed using a Mouse High Sensitivity T-Cell 18-Plex Discovery Assay Array (Eve Technologies Corp., MDHSTC18). Heat maps of differentially expressed cytokines or chemokines were generated using Morpheus.

Single-cell sequencing

Bone marrow and peripheral blood were collected from mice carrying orthotopic PyMT-N tumors (C57BL/6, Envigo), using previously described methods (29). RNA isolated from Hematopoietic cells using 10X Genomics Chromium protocol was subjected to single-cell RNA sequencing. The 10X Genomics Chromium system was used for library preparation and libraries were prepared per 10x Genomics guidelines. Sequencing adapters are provided by 10x Genomics. All sequencing results were pooled from three mice (three technical replicates). Raw sequencing files were imported into the 10x Genomics Cell Ranger toolkit (v3.1.0) for alignment, filtering, barcode counting, and UMI counting with default parameters. The mm10 (v3.0.0) genome was used for reads mapping. The Seurat (v3.2.3) package on R (v4.0.2) was used for downstream analysis. For quality control, we kept cells with less than 20,000 read counts and have less than 10% mitochondria genes. These parameters aimed to filter doublets and dead cells. We then filtered mitochondrial genes (genes start with mt), ribosomal protein genes (genes start with Rpl and Rps), and unspecified genes (genes start with Gm). Next, we used the SCTransform function in the Seurat package, which implemented regularized negative binomial regression to normalize raw Unique Molecular Identifier (UMI) counts. Variable genes identified by this method were used as inputs for principal component analysis (PCA). We applied Uniform Manifold Approximation and Projection analysis for visualization using the first 50 principal components identified by PCA. Cells were clustered by the shared nearest neighbor with the FindNeighbors and FindClusters functions in the Seurat package. Matured neutrophils are identified by expression of Ly6g, Camp, Ltf, and S100a9. Various clusters were ordered in pseudo-time using the Monocle 3 package (v1.0.0). In blood, two neutrophil clusters were identified, one before infiltration of tumors and the other after tumor infiltration according to pseudo-time, and were defined as "pre-" and "posttumor" clusters. The difference in *Malat1* RNA expression of neutrophils before entering the tumor and neutrophils after exiting the tumor was visualized by a violin plot generated by Vlnplot function in Seurat package. The *P* value was calculated by FindAllMarkers function in Seurat package using a Wilcoxon Rank-Sum test. Single-cell sequencing data generated in this study are publicly available in Gene Expression Omnibus (GEO) using the accession number GSE222854.

Statistical analysis

Sample sizes for treatment studies were determined from preliminary short-term studies and availability of ASO, not statistically predetermined. All graphs and statistical analysis were performed using GraphPad Prism 9.4.1 (GraphPad Prism, RRID:SCR_002798). Two-way ANOVA with the Šídák's multiple comparisons test were used to determine significant differences in tumor volumes over time. Kaplan–Meier curves with Log-Rank (Mantel–Cox) test were used to determine change in survival between treatment groups. For all comparisons between two experimental groups an unpaired two-tailed Student *t* test was used. In grouped analysis, multiple Student *t* tests using the Holm–Šídák method were used and the *P* value was adjusted for multiple comparisons. With three or more experimental groups significance was determined using one-way ANOVA and Dunnett's multiple comparisons test with an adjusted *P* value for multiple comparisons. A P value of <0.05 was considered significant.

Data availability

Single-cell sequencing data generated in this study are publicly available in GEO using the accession number GSE222854. For flow cytometry studies, raw data were generated at Baylor College of Medicine Cytometry and Cell Sorting Core. Derived data supporting the findings of this study are available from the corresponding author upon request. Other data generated in this study are available upon request from the corresponding author or can be found in the article and its Supplementary Files.

Results

Single-agent Malat1 ASO delays primary tumor growth in TNBC preclinical mouse models

To determine the effect of *Malat1* inhibition on mammary tumor progression *in vivo*, we used the established syngeneic *Tp53*-null

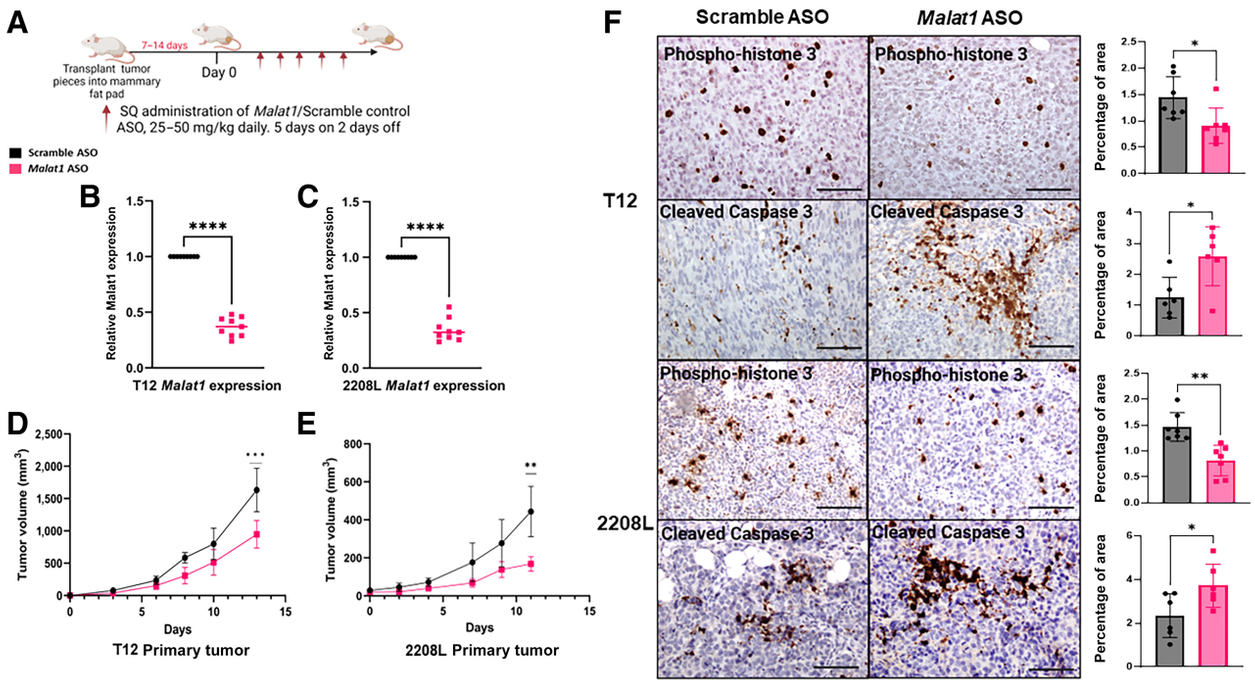

Figure 1.

Single-agent *Malat1* ASO delays primary tumor growth in the TNBC preclinical mouse model. **A,** Experimental design of treatment study. WT BALB/c mice had T12 or 2208 L tumor pieces implanted into the mammary fat pad and were treated with either Scramble ASO or *Malat1* ASO once tumor was palpable (≤50 mm^3). **B** and **C,** qPCR analysis of RNA extracted from tumors display significant decrease of *Malat1* expression in the *Malat1* ASO treatment group. Relative fold change based on *Gapdh* RNA level. Error bars represent standard deviation (SD), ****, $P < 0.0001$ using the two-tailed unpaired Student *t* test. **D** and **E,** Tumor growth curves of T12 and 2208 L mice treated with Scramble ASO ($n = 9$) and *Malat1* ASO ($n = 9$). Data points represented as the mean ± SD. **, $P < 0.01$; ***, $P < 0.001$ by two-way ANOVA and Sidak's multiple comparisons test. Treatment studies were performed once in T12 tumor and twice in 2208 L tumors. **F,** Representative IHC images of tumor sections stained for Phospho-histone 3 and Cleaved Caspase 3; scale bar, 80 μm. Quantifications of positive area of tumor sections using ImageJ using the geometric mean of 3 representative images from each tumor section, 6–7 tumor sections were used for each treatment group. Error bars represent SD, ****, $P < 0.0001$ using the two-tailed unpaired Student *t* test.

mouse models derived from BALB/c mice that recapitulate the aggressive and heterogenous nature of TNBC (28). The neutrophil-enriched 2208 L luminal-like tumor subtype and macrophage-enriched T12 and T11 Claudin-low tumor subtypes were used because of their highly immunosuppressive myeloid compartments, which contribute to both tumorigenesis, metastasis, and resistance to available treatments (29). Gapmer ASOs allow for targeted degradation of *Malat1* and have been shown to achieve knockdown with great efficiency in previous studies (22). WT BALB/c mice had *Tp53*-null tumor pieces implanted into the mammary fat pad and once palpable, either a *Malat1*-targeted ASO or a scramble control ASO was injected subcutaneously for five continuous days with a 2-day drug holiday (**Fig. 1A**). After 5 days of treatment, the *Malat1* ASO caused an approximately 60%–75% depletion of *Malat1* RNA expression that was maintained using the 5 days on 2 days off treatment regimen (**Fig. 1B** and **C**). Similarly, tumor-derived cell lines treated with *Malat1* ASO for 48 hours had a significant decrease of *Malat1* RNA expression (Supplementary Fig. S1C–S1E). *Malat1* inhibition led to a delay in primary tumor growth for both T12 and 2208 L tumors, and after 14 days of treatment the tumor volume was significantly reduced in both models (**Fig. 1D** and **E**). In longer treatment studies with 2208 L and T11, *Malat1* inhibition maintained delayed tumor progression as well as slightly prolonged survival in 2208 L tumor-bearing mice (Supplementary Fig. S1F–S1H). To ensure *Malat1*-specific knockdown, expression of a similar abundant lncRNA *Neat1* was quantified and there was no significant change in both Claudin-low and luminal-like tumor subtypes (Supplementary Fig. S1I and S1J). There was no significant change in weight with mice undergoing ASO treatment in either tumor models (Supplementary Fig. S1K and S1L). IHC staining of tumor sections after harvest revealed that *Malat1* ASO–treated tumors had decreased staining of the proliferative marker phospho-histone 3 and increased apoptosis, as evident by increased cleaved caspase 3 staining (**Fig. 1F**). These results demonstrate that specifically targeting *Malat1* using an ASO and subsequent *Malat1* inhibition results in decreased tumor volume due to increased cell death coupled with decreased cell proliferation.

Malat1 inhibition decreases the immunosuppressive myeloid cells in the TME

Malat1 has previously been shown to contribute to cancer progression by increasing both tumor cell proliferation and invasion (33, 34), but little is known about its effect on the TIME. To study changes to the TIME with *Malat1* knockdown, TILs were isolated from T12 and 2208 L tumors treated with *Malat1* ASO for 14 days and myeloid cell markers were quantified using flow cytometry (**Fig. 2A** and **E**; Supplementary Fig. S2A and S2B). *Malat1*-depleted T12 Claudin-low tumors, which are highly macrophage enriched, displayed a decrease in $F4/80^+$ macrophages. In addition, of the macrophages present, there

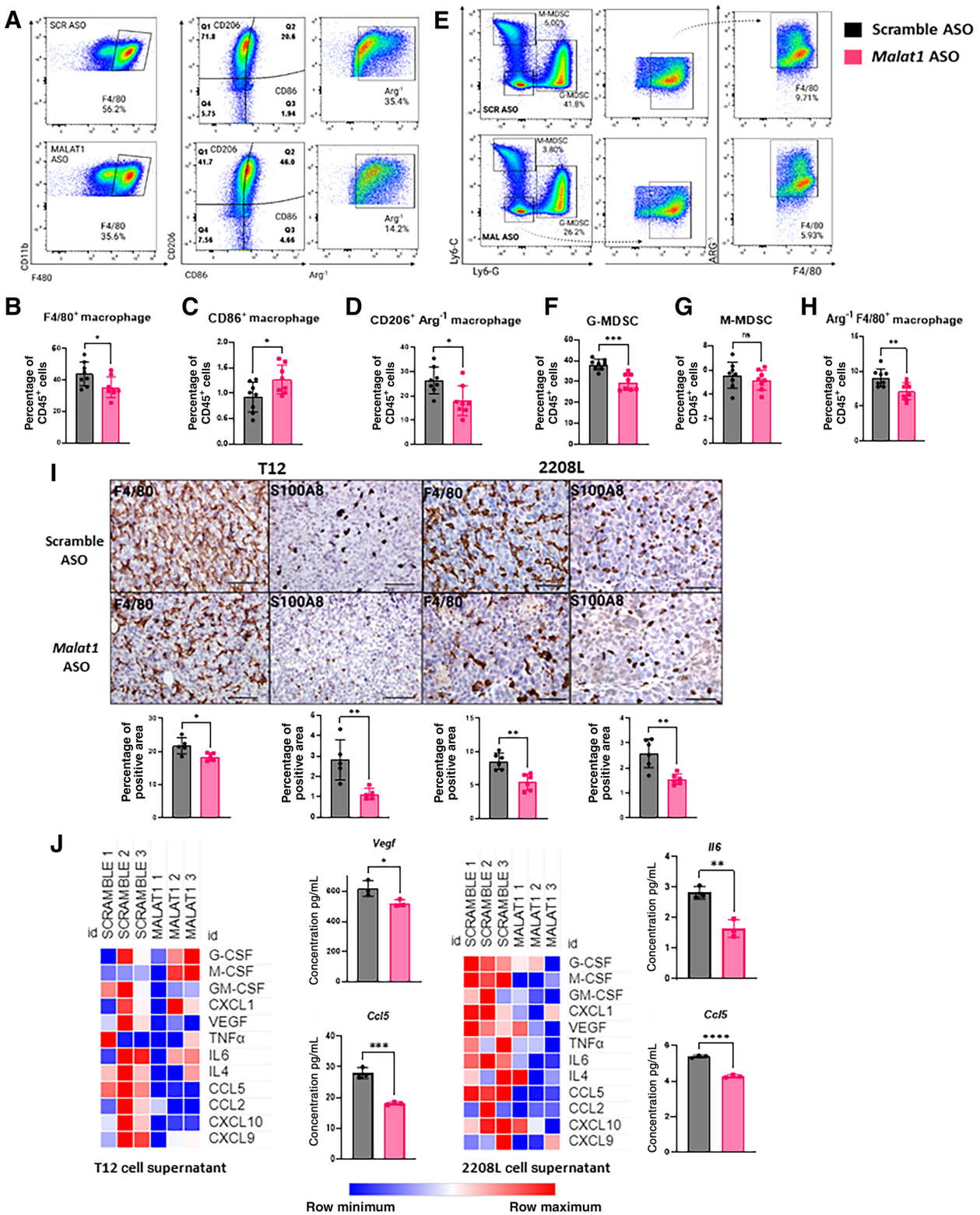
A
SCR ASO
F4/80
56.2%
MALAT1
ASO
F4/80
35.6%
CD11b
F480
Q1 CD206
71.8
Q2
20.6
Q4
5.75
CD86
Q3
1.94
Arg-1
35.4%
Q1 CD206
41.7
Q2
46.0
Q4
7.56
CD86
Q3
4.46
Arg-1
14.2%
CD206
CD86
Arg-1
E
M-MDSC
6.00%
G-MDSC
41.8%
SCR ASO
F4/80
9.71%
M-MDSC
3.80%
G-MDSC
26.2%
MAL ASO
F4/80
5.93%
Ly6-C
Ly6-G
ARG-1
F4/80
Scramble ASO
Malat1 ASO
B
F4/80+ macrophage
C
CD86+ macrophage
D
CD206+ Arg-1 macrophage
F
G-MDSC
G
M-MDSC
H
Arg-1 F4/80+ macrophage
Percentage of CD45+ cells
I
T12
2208L
F4/80
S100A8
Scramble ASO
Malat1 ASO
Percentage of positive area
J
SCRAMBLE 1
SCRAMBLE 2
SCRAMBLE 3
MALAT1 1
MALAT1 2
MALAT1 3
id
G-CSF
M-CSF
GM-CSF
CXCL1
VEGF
TNFα
IL6
IL4
CCL5
CCL2
CXCL10
CXCL9
T12 cell supernatant
2208L cell supernatant
Vegf
Il6
Ccl5
Concentration pg/mL
Row minimum
Row maximum

was a decrease in $CD206^+$Arginase-1 (Arg-1)$^+F4/80^+$ cells, which are representative of immunosuppressive "M2-like" macrophages (**Fig. 2B** and **D**) Conversely, there was slight increase in $CD86^+F4/80^+$ cells with CD86 being an inflammatory marker present on "M1-like" macrophages (**Fig. 2C**). In 2208 L tumors, which are highly neutrophil enriched, *Malat1* inhibition led to a decrease in $Cd11b^+Ly6C^{low}Ly6G^{high}$ cells known as granulocytic MDSCs (G-MDSC), which are the most abundant granulocytes present (**Fig. 2F**). The monocytic MDSC (M-MDSC) compartment characterized by $Cd11b^+Ly6C^{high}Ly6G^{low}$ showed no significant difference between treatment groups (**Fig. 2G**). Previous studies have shown that when one myeloid population is depleted, there may be a compensatory enrichment in a separate myeloid population (29), but with the *Malat1* ASO treatment, we observed a decrease in Arg-1^+ macrophages in 2208 L tumors as well (**Fig. 2H**). Tumor sections were stained with F4/80 and the neutrophil marker S100a8 to elucidate the spatial distribution of the myeloid cells. IHC revealed myeloid cells to be widely dispersed throughout the tumor with an abundance of macrophages present in T12 tumors and more neutrophils in 2208 L tumors, as expected. *Malat1*-depleted tumors had decreased staining of both F4/80 and S100a8 (**Fig. 2I**) in both tumor models.

To determine tumor-intrinsic effects that might contribute to decreased myeloid populations, tumor-derived T12 and 2208 L cell lines were treated with *Malat1* ASO and the supernatants were collected for analysis using an inflammatory cytokine/chemokines array. *Malat1* depletion in both cell lines altered the tumor secretory profiles. In T12 cancer cells, there was a decrease in chemokines known to recruit immunosuppressive macrophages and neutrophils to the tumor site (ref. 35; including a significant decrease in Ccl5; **Fig. 2J**). The inflammatory chemokines, Cxcl9 and Cxcl10 that help to recruit "M1-like" macrophages to the TME, were also decreased in *Malat1* ASO–treated tumor cells providing evidence that *Malat1* inhibition in tumor cells is not responsible for repolarizing macrophages to a more inflammatory phenotype. *Malat1* ASO–treated 2208 L tumor cells had decreased secretion of immunosuppressive cytokines/chemokines similar to T12. Chemokines Cxcl1, Gm-csf, and Tnfα were reduced along with a significant decrease in Ccl5 and the cytokine IL6. These factors are known to bolster the recruitment and development of MDSCs (35–37) and support immunosuppression. Vegf, a promoter of angiogenesis and myeloid cell enrichment (36), was decreased in both cell lines (**Fig. 2J**). These analyses reveal that *Malat1* inhibition reduces the frequency of immunosuppressive immune cells found in the TNBC microenvironment with concordant changes to the tumor cell's secretory profile resulting in decreased recruitment of myeloid cells to the primary tumor. However, because neither myeloid compartment was completely abolished, we next examined the function of the remaining myeloid cells present.

Malat1 inhibition decreases TAM and MDSC-immunosuppressive function

After establishing that *Malat1* depletion in tumor cells can influence the recruitment of immunosuppressive myeloid cells to the TME, we next wanted to understand the effect that *Malat1* inhibition had on TAM and MDSC function. Both TAMs and MDSCs extracted from T12 and 2208 L tumors, respectively, were found to have abundant *Malat1* RNA expression comparable with tumor cells (Supplementary Figs. S3B and S4A). Single-cell sequencing studies showed that neutrophils collected from peripheral blood mononuclear cells before and after direct tumor cell contact displayed increased expression of *Malat1* once encountering the tumor (Supplementary Fig. S4B), suggesting that *Malat1* may play a role in the tumor education of neutrophils. This led us to take a more detailed look at the intrinsic effect that *Malat1* depletion may have on myeloid cells. To determine whether the *Malat1* ASO was able to efficiently knockdown *Malat1* in TAMs isolated from T12 primary tumors and MDSCs isolated from 2208 L primary tumors, were cultured *in vitro* for 72 hours (Supplementary Figs. S3A and S4C) in the presence of 250 nmol/L ASO. In both cell types, *Malat1* RNA expression was significantly decreased *in vitro* (**Figs. 3A** and **4A**). In addition, TAMs extracted from T12 tumors (**Fig. 3B**) and MDSCs extracted 2208 L tumors (**Fig. 4B**) after 5 days of ASO treatment showed significant knockdown of *Malat1* RNA expression confirming that this treatment regimen reduced *Malat1* expression in myeloid cells as well as tumor cells. To determine changes in TAM function, TAMs isolated from T12 tumors were cultured *in vitro* with CD3/CD28-stimulated T cells isolated from the spleen of a WT BALB/c mouse. The ASO concentration of 250 nmol/L caused a 60% to 80% knockdown in TAMs (Supplementary Fig. S3C) but not in T cells (Supplementary Fig. S3D), and there was no change in proliferation when T cells were cultured alone with this concentration of ASO. T cells cultured with *Malat1*-depleted TAMs for 72 hours had increased cell proliferation, as evidenced by decreased CFSE expression (**Fig. 3C** and **D**; Supplementary Fig. S3E), with a significant increase in $CD8^+$ T-cell proliferation and no change in $CD4^+$ T-cell proliferation (**Fig. 3E** and **F**). Similarly, when MDSCs isolated from 2208 L tumors with decreased *Malat1* RNA expression were co-cultured with activated T cells, $CD8^+$ T-cell proliferation increased (**Fig. 4C–F**; Supplementary Fig. S4D). To assess the effect that *Malat1*-depleted myeloid cells had on T-cell killing capability, TAMs or MDSCs isolated from a T12 primary tumor were cultured with a GFP-labeled T12 tumor-derived cell line, and GFP-specific T cells isolated from the spleen of JEDI mouse at 1:1:1 and 5:5:1 T-cell:TAM: tumor cell ratios and a 1:1:1 T-cell:MDSC:tumor cell ratio in the presence of 250 nmol/L ASO. Pictures and the GFP signal of cells were taken every 2 hours using Incucyte (**Figs. 3G** and **4G**). Residual cells were analyzed using flow cytometry (Supplementary Fig. S3F) and

Figure 2.

Malat1 inhibition decreases immunosuppressive myeloid cells in the TME. **A,** Gating strategy was used to identify macrophages in the TILs of T12 tumors using FlowJo 10.8.1. **B–D,** Flow cytometry quantification of macrophage populations as the percentage of $CD45^+$ cells using GraphPad Prism 9.4.1. Eight tumors used for each treatment group. Error bars represent standard deviation (SD). *, $P < 0.05$; **, $P < 0.01$; ***, $P < 0.001$ using the two-tailed unpaired Student *t* test. **E,** Gating strategy used to identify neutrophils in the TILs of 2208 L tumors using FlowJo 10.8.1. **F–H,** Flow cytometry quantification of myeloid populations as the percentage of $CD45^+$ populations using GraphPad Prism 9.4.1. Error bars represent SD. *, $P < 0.05$; **, $P < 0.01$; ***, $P < 0.001$ using the two-tailed unpaired Student *t* test. Eight tumors were used in each treatment group. The experiment was performed once with T12 primary tumors and twice with 2208 L primary tumors. **I,** Representative IHC images of tumor sections stained for F4/80 and S100a8; scale bar, 80 μm. Quantifications of positive area of tumor sections using ImageJ using the geometric mean of up to 3 representative images from each tumor section ($n = 5$–6 tumors). Error bars represent SD. *, $P < 0.05$; **, $P < 0.01$; ***, $P < 0.001$ using the two-tailed unpaired Student *t* test. **J**, Heat map of cytokine/chemokine array of supernatants collected from 2208 L and T12 tumor-derived cell lines after *Malat1 k*nockdown. Quantification of immunosuppressive cytokine/chemokines. Error bars represent SD. *, $P < 0.05$; **, $P < 0.01$; ****, $P < 0.0001$ using the two-tailed unpaired Student *t* test.

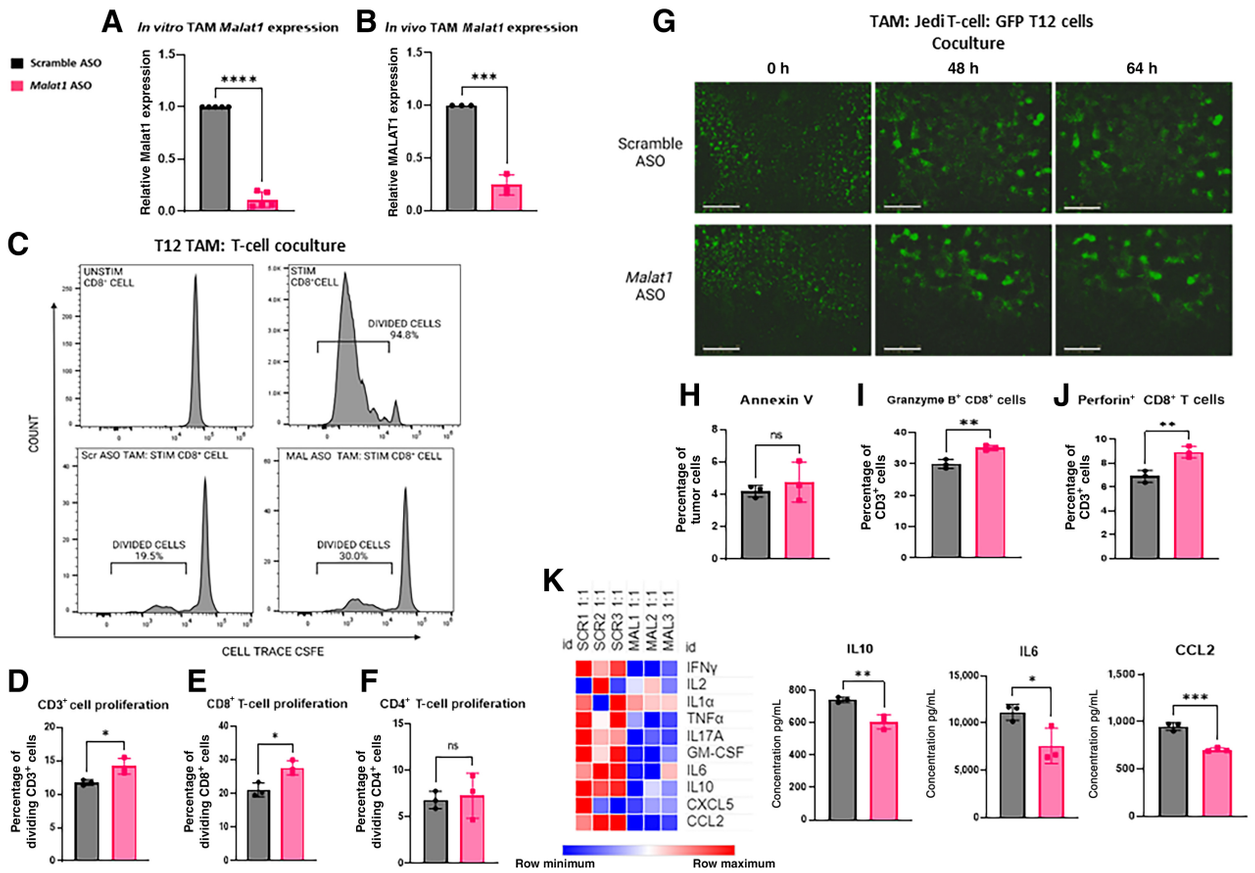

Figure 3.

Malat1 inhibition decreases TAM-immunosuppressive function. **A,** qPCR analysis of RNA extracted from TAMs extracted from a T12 primary tumors and cultured *in vitro* for 72 hours with 250 nmol/L ASO of Scramble/*Malat1* ASO displays significant decrease of *Malat1* RNA expression in the *Malat1* ASO treatment group. Relative fold change based on *Gapdh* RNA level. Error bars represent standard deviation (SD), ****, $P < 0.0001$ using the two-tailed unpaired Student *t* test. Data are representative of 3 independent experiments. **B**, qPCR analysis of RNA extracted from isolated TAMs extracted from a T12 primary tumor after 5 days of subcutaneous treatment displays significant decrease of *Malat1* expression in the *Malat1* ASO treatment group. Relative fold change based on *Gapdh* RNA level. Error bars represent SD, ***, $P < 0.001$ using the two-tailed unpaired Student *t* test. **C,** Representative proliferation plots of isolated TAMs from T12 primary tumors cultured with T cells collected from naïve splenocytes of BALB/c mice and stained with CFSE and activated with CD3/CD28 Dynabeads at 0.5:1 TAM:T-cell ratio. Stained unstimulated control and stained stimulated T cells without TAMs were used to create appropriate gates. **D–F,** Flow cytometry quantification of $CD3^+$, $CD8^+$, and $CD4^+$ T cells after 72 hours coculture with *Malat1*-depleted TAMs as the percentage of parent population. Experimental $n = 3$. Error bars represent SD, *, $P < 0.05$ using the two-tailed unpaired Student *t* test. **G,** Representative Incucyte images of the GFP-labeled T12 tumor-derived cell line cultured with isolated TAMs from a T12 primary tumor and GFP-specific T cells isolated from the splenocytes of a WT JEDI mouse at a 1:1:1 ratio. A total of 5,000 tumor cells were plated 24 hours before the addition of TAMs and T cells; scale bar, 800 μm. Images were taken at 0, 48, and 64 hours. Experimental $n = 2$. **H** and **I**, Flow cytometry quantification of Annexin V^+ tumor cells and quantification of Granzyme B^+ and Perforin$^+$ T cells after 72 hours. Error bars represent SD. *, $P < 0.05$; **, $P < 0.01$; ***, $P < 0.001$ using the two-tailed unpaired Student *t* test. **K,** Heat map of cytokine/chemokine array of supernatant collected from cocultures with *Malat1*-depleted TAMs, GFP-labeled tumor, and GFP-specific T cells at a 1:1 TAM:T-cell ratio, where 25,000 TAMs and 25,000 T cells were added to wells containing 5,000 GFP positive tumor cells. Quantification of key immunosuppressive cytokine/chemokines. Error bars represent SD. *, $P < 0.05$; **, $P < 0.01$; ***, $P < 0.001$ using the two-tailed unpaired Student *t* test.

there was no change in the cell death marker, Annexin V, in *Malat1* ASO–treated TAM cocultures (**Fig. 3H**). T cells were also collected and analyzed (Supplementary Fig. S3G), and we observed an increase in $CD8^+$ cells with the cytotoxic T-cell markers Granzyme B and Perforin (**Fig. 3I** and **J**). *Malat1*-depleted MDSC cocultures had increased T-cell cytotoxicity, as evidenced by a significant increase in Annexin V^+ tumor cells as well as an increase in both Granzyme B^+CD8^+ T cells and Perforin$^+CD8^+$ T cells (**Fig. 4H–J**). TAMs and MDSCs were also cultured with tumor cells without T cells as additional controls (Supplementary Figs. S3H and S4E). A chemokine/cytokine assay of supernatants collected in the 5:5:1 ratio for TAM and the 1:1:1 ratio for MDSC cocultures displayed a secretory profile similar to tumor cells where a decrease in immunosuppressive chemokines was observed, and in cocultures of both cell types there was a significant decrease in Il10 (**Figs. 3K** and **4K**). In the presence of tumor cells, a decrease in Ifnγ secretion in *Malat1* ASO–treated cultures was also observed, suggesting that *Malat1* inhibition decreased the overall inflammatory signature in TAMs and MDSCs, which included a decrease in immunosuppressive factors. These results indicate a change in functionality of myeloid cells with *Malat1* knockdown in TNBC. Furthermore, *Malat1* inhibition within the primary TNBC TME helped to create a more immunostimulatory environment by decreasing the suppressive effects of TAMs and MDSCs on T cells, which may then allow for an increased T-cell response. These results

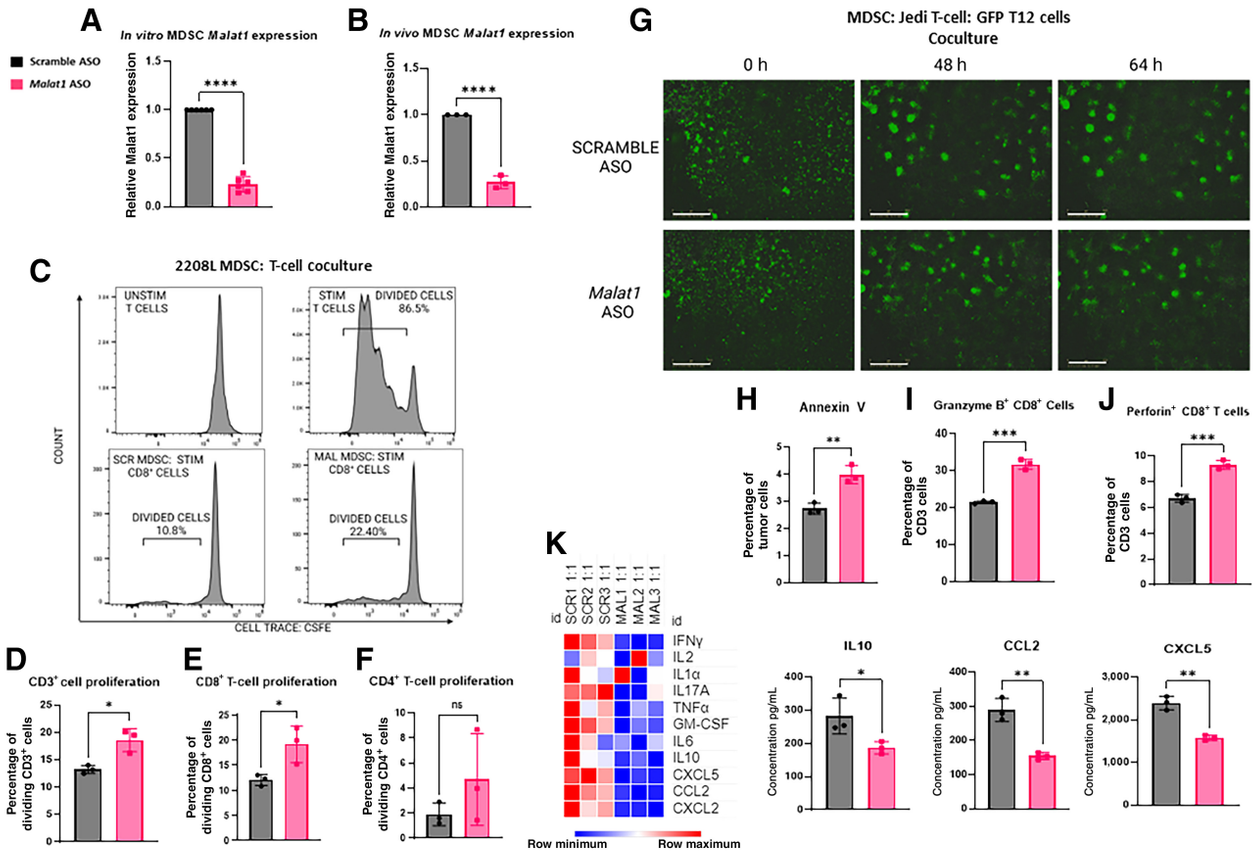

Figure 4.

Malat1 inhibition decreases MDSC-immunosuppressive function. **A,** qPCR analysis of RNA extracted from GR1$^+$ cells, extracted from a 2208 L primary tumor, and cultured *in vitro* for 72 hours with 250 nmol/L of Scramble/*Malat1* ASO displays significant decrease of *Malat1* expression in the *Malat1* ASO treatment group. Relative fold change based on GAPDH RNA level. Error bars represent standard deviation (SD) ****, $P < 0.0001$ using the two-tailed unpaired Student *t* test. **B,** qPCR analysis of RNA extracted from isolated Gr1$^+$ cells from 2208 L primary tumors after 5 days of subcutaneous ASO treatment displays significant decrease of *Malat1* expression in the *Malat1* ASO treatment group. Relative fold change based on *Gapdh* RNA level. Error bars represent SD, ***, $P < 0.001$ using the two-tailed unpaired Student *t* test. **C,** Representative proliferation plots of isolated MDSCs from 2208 L primary tumors cultured with T cells isolated from naïve splenocytes of BALB/c mice and stained with CFSE and activated with CD3/CD28 Dynabeads at 0.5:1 MDSC:T-cell ratio. 25,000 2208 L tumor cells were added to culture to improve MDSC cell viability. Stained unstimulated control and stained stimulated T cells without MDSCs were used to create appropriate gates. **D–F,** Flow cytometry quantification of CD3$^+$, CD8$^+$, and CD4 $^+$ T cells as the percentage of parent population after 72 hours coculture with *Malat1*-depleted MDSCs. Experimental $n = 2$. Error bars represent SD, *, $P < 0.05$ using the two-tailed unpaired Student *t* test. **G,** Representative Incucyte images of GFP-labeled T12 tumor-derived cell line cultured with isolated Gr1$^+$ cells isolated from a T12 primary tumor and GFP-specific T cells isolated from the splenocytes of a WT JEDI mouse at a 1:1:1 ratio. A total of 5,000 tumor cells were plated 24 hours before the addition of MDSCs and T cells; scale bar, 800 μm. Images were taken at 0, 48, and 64 hours. **H–J,** Flow cytometry quantification of Annexin V$^+$ tumor cells and quantification of Granzyme B$^+$ and Perforin$^+$ T cells after 72 hours. Error bars represent SD. *, $P < 0.05$; **, $P < 0.01$; ***, $P < 0.001$ using the two-tailed unpaired Student *t* test. **K,** Heat map of cytokine/chemokine array of supernatant collected from cocultures with *Malat1*-depleted MDSCs, GFP-labeled tumor cells, and GFP-specific T cells at a 1:1 MDSC:T-cell ratio where a total of 5,000 MDSCs and 5,000 T cells were added to wells containing 5,000 GFP-positive tumor cells. Quantification of key immunosuppressive cytokine/chemokines. Error bars represent SD. *, $P < 0.05$; ***, $P < 0.001$ using the two-tailed unpaired Student *t* test.

led us to examine the effects on T cells within the TME after *Malat1* ASO treatment.

Malat1 inhibition increases T-cell infiltration in the TME

Once we established the effect *Malat1* knockdown had on myeloid populations in the TME, we wanted to investigate the effect *Malat1* depletion had on T-cell infiltration using TILs isolated from T12 and 2208 L primary tumors and quantified using flow analysis (**Fig. 5A**; Supplementary Fig. S5A). In 2208 L tumors, we observed a significant increase in CD8$^+$ T cells with a greater population of CD8$^+$ T cells expressing the cytotoxic markers Granzyme B and Ifnγ (**Fig. 5B–D**). There was also a decrease in the CD4$^+$ T-cell population, which coincided with a significant decrease in immunosuppressive regulatory Foxp3$^+$CD4$^+$ T cells (Tregs, regulatory T-cell; **Fig. 5E** and **F**). In T12 tumors there was a significant increase in Granzyme B$^+$ T-cell infiltration, with no change in overall CD8$^+$ T-cell infiltration (**Fig. 5G** and **H**). T12 tumors contained a much smaller population of CD4$^+$ T cells and no significant change in Tregs was observed (**Fig. 5I** and **J**). We performed CD8α and Foxp3 IHC staining of tumor sections to determine the spatial distribution of these cells. Many T cells were found in the stroma of 2208 L tumors (Supplementary Fig. S5B), although *Malat1* ASO–treated tumors showed an increase in CD8α staining, with more cells found outside of the stroma as compared with Scramble ASO–treated tumors (**Fig. 5K**). T12 tumors

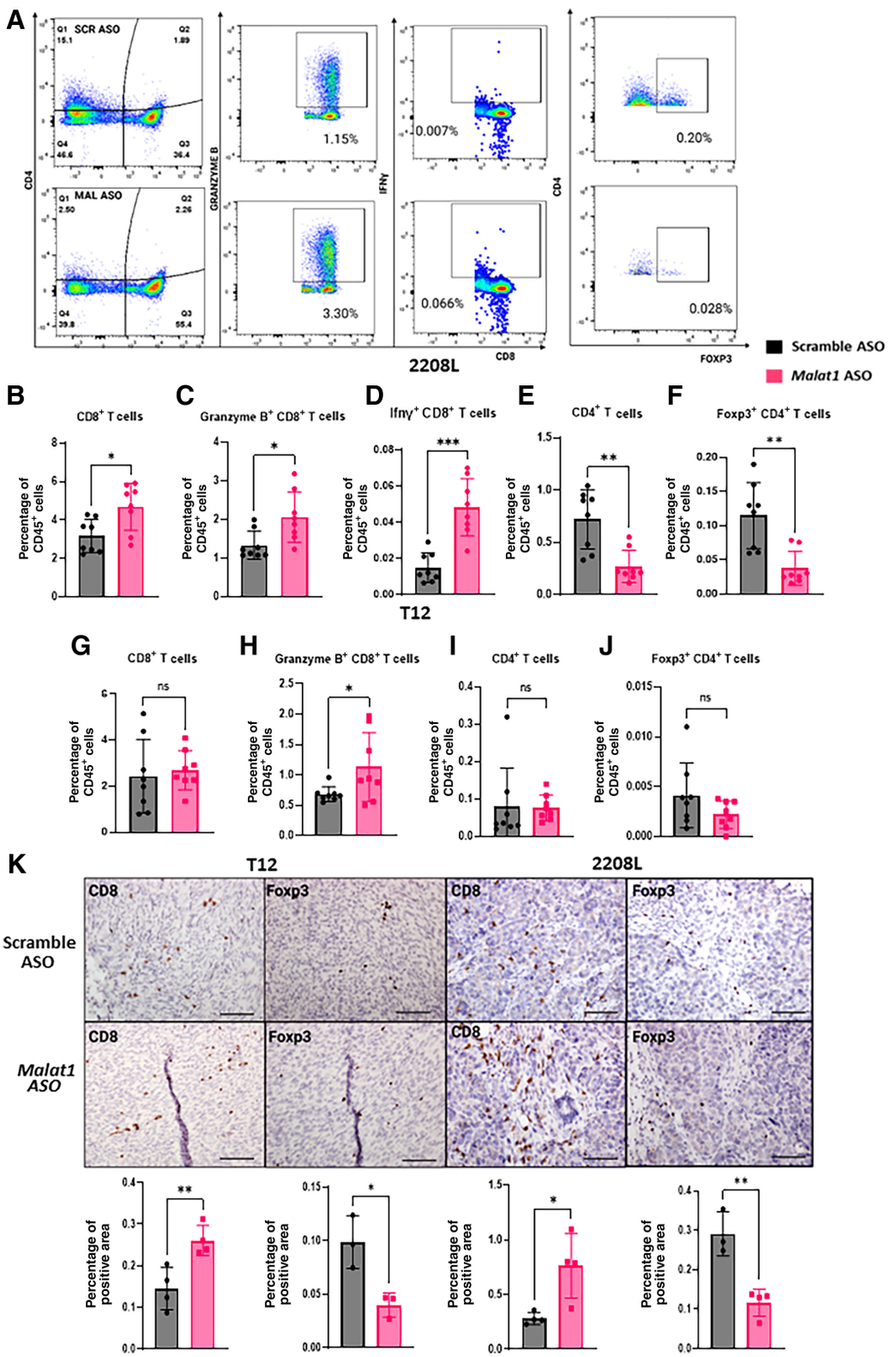
A
Q1 SCR ASO
Q2 1.89
Q4 46.6
Q3 36.4
Q1 MAL ASO
Q2 2.26
Q4 39.8
Q3 55.4
CD4
GRANZYME B
1.15%
3.30%
IFNγ
0.007%
0.066%
CD8
CD4
0.20%
0.028%
FOXP3
2208L
Scramble ASO
Malat1 ASO
B
CD8+ T cells
C
Granzyme B+ CD8+ T cells
D
Ifnγ+ CD8+ T cells
E
CD4+ T cells
F
Foxp3+ CD4+ T cells
Percentage of CD45+ cells
T12
G
CD8+ T cells
H
Granzyme B+ CD8+ T cells
I
CD4+ T cells
J
Foxp3+ CD4+ T cells
ns
K
T12
2208L
Scramble ASO
Malat1 ASO
CD8
Foxp3
Percentage of positive area

also displayed a slight increase in CD8α staining in *Malat1* ASO–treated tumors compared with Scramble (**Fig. 5K**). Foxp3 staining was quite sparse, however, quantification revealed a decrease in Foxp3 with *Malat1* ASO treatment in both tumor models (**Fig. 5K**). This analysis of primary tumor TILs helps to support the conclusion that *Malat1* inhibition creates a more immunostimulatory TME with increased cytotoxic T-cell infiltration. To determine the extent the increased immunostimulatory TME after *Malat1* depletion had on tumor progression, we performed a series of treatment studies in T cell–deficient mice. 2208 L tumor pieces were implanted into the mammary fat pad of Nude athymic mice that do not have $CD8^+$ or $CD4^+$ T cells and treated with either *Malat1* ASO or Scramble control. In this T cell–deficient model, there was no change in tumor growth between treatment groups even though *Malat1* expression was significantly reduced with ASO treatment (Supplementary Fig. S5C and S5D). A pilot study using a CD8α-specific antibody that successfully ablated circulating $CD8^+$ T cells (Supplementary Fig. S5E) also showed no significant change in primary tumor growth between treatment groups while still significantly decreasing *Malat1* RNA expression in the tumor. Conversely, mice treated with IgG and *Malat1* ASO had a decreased tumor volume, although due to small sample size, this was not statistically significant (Supplementary Fig. S5F–S5H). These results underscore the importance of the TME in tumor response in our mouse models, and that altering the immune microenvironment, in particular increasing T-cell infiltration, is enough to delay tumor progression.

Malat1 inhibition in T cells increases proliferation and cell cytotoxicity

Although there was an increase in Ifnγ in the tissue homogenate samples, *Malat1* depletion in T12 and 2208 L tumor cells did not increase immunostimulatory cytokine secretion from cells (Supplementary Fig. S6A and S6B). This led us to investigate whether the increase in cytotoxic T-cell infiltration observed *in vivo* may be caused, in part, by intrinsic changes to the T cells. To study the effect of *Malat1* depletion on T cells, we used *in vitro* culture and coculture experiments. $CD3^+$ T cells were isolated from the spleen of WT BALB/c mice through negative selection and stimulated with CD3/CD28 activation beads for 3 to 5 days. *Malat1* and Scramble ASOs (500 nm each) were added to wells on days 2 and 4 of culture. The ASO concentration used could effectively reduce Malat1 expression by at least 50% (Supplementary Fig. S6C). qPCR analysis revealed significant knockdown of *Malat1* RNA expression with a greater depletion of *Malat1* after 5 days of culture when T cells were treated twice with the ASO (**Fig. 6A**). To determine the effects of *Malat1* knockdown on T-cell proliferation, T cells were stained with CFSE before being seeded. After 3 days, we observed reduced CFSE in *Malat1* ASO–treated T cells as compared with the Scramble ASO–treated T cells (**Fig. 6B**; Supplementary Fig. S6D) signifying increased proliferation. Flow analysis of *Malat1*-depleted T cells cultured for 3 to 5 days showed a slight increase in $CD8^+$ T-cell populations after 3 days of culture with the difference being less pronounced after 5 days (**Fig. 6C**). When examining cytotoxic markers, we saw a modest increase in Granzyme B^+ and $Perforin^+$ $CD8^+$ cells after 3 days that was maintained after 5 days in culture (**Fig. 6D** and **E**).

To further investigate the effect of *Malat1* inhibition on cell cytotoxicity, GFP-specific T cells isolated from the splenocytes of a WT JEDI mouse were cultured with GFP-labeled T12 cells at a 1:1 and 5:1 effector: target ratio for approximately 48 hours and monitored using Incuyte. At the 1:1 effector ratio, residual tumor cells were analyzed and Annexin V^+ tumor cells were quantified. At the 5:1 effector ratio, there was a negligible amount of residual tumor cells collected so we chose to assess cell cytotoxicity by measuring the remaining GFP signal in each well. *Malat1*-depleted T cells showed increased tumor cell killing and a slight increase in Granzyme B and Perforin cytotoxic markers at the 5:1 ratio (**Fig. 6F–J**). Cocultures not treated with ASO, along with T cells cultured alone and tumor cells cultured alone were all used as control groups (Supplementary Fig. S6E and S6F). A cytokine assay of supernatant collected from these cocultures revealed that *Malat1* ASO–treated T cells had increased inflammatory cytokine secretions, including an increase in Ifnγ and Tnfα that was not seen in tumors or myeloid cells. Unlike in the myeloid-cell populations, there were no significant changes in immunosuppressive cytokine/chemokine secretion (**Fig. 6K**). These findings highlight the potential of improving T-cell cytotoxicity through *Malat1* inhibition while also emphasizing the different role that *Malat1* plays in effector T cells as compared with myeloid and tumor cells. An increase in inflammation was observed in T cells that was not seen in TAMs, MDSCs, or tumor cells. T cells treated with the *Malat1* ASO could potentially be used in an *ex vivo* setting to improve therapeutic response.

Combination of Malat1 ASO with chemotherapy or ICB improves response in preclinical mouse models

The promising effects that the single-agent *Malat1* ASO treatment had on 2208 L and T12 tumors, particularly the increased immunostimulatory effect seen in the TIME, led us to investigate potential benefit of combining the ASO with established clinical therapies such as chemotherapy and ICB. BALB/c mice implanted with 2208 L tumors were randomized into four separate treatment cohorts: Carboplatin at half the clinically relevant dose of 25 mg/kg with Scramble ASO, 25 mg/kg of carboplatin with *Malat1* ASO, 10 mg/kg anti-PD1 with Scramble ASO, and 10 mg/kg anti-PD1 with *Malat1* ASO. A small cohort of mice was treated with isotype-matched IgG antibody alone as a separate control for the ICB treatment groups. Mice were treated using an established treatment regimen (**Fig. 7A**). We observed that in both combination treatment groups there was a significant delay in primary tumor growth and tumor volume with a significant reduction of tumor weights at time of harvest (**Fig. 7B** and **C**). Although we did not achieve tumor stasis or regression with combination treatments, we were

Figure 5.

*Malat1 i*nhibition increases T-cell infiltration in the TME. **A,** Gating strategy used to identify cytotoxic $CD8^+$ T cells and regulatory $CD4^+$ T cells in the TILs of 2208 L tumors using FlowJo 10.8.1. **B–J,** Flow cytometry quantification of T cells as the percentage of $CD45^+$ populations in 2208 L and T12 tumors using GraphPad Prism 9.4.1. Error bars represent standard deviation (SD), *, $P < 0.05$; **, $P < 0.01$; ***, $P < 0.001$ using the two-tailed unpaired Student *t* test. Eight tumors were used for each treatment group. The experiment was performed once with T12 primary tumors and twice with 2208 L primary tumors. **K**, Representative IHC images of tumor sections stained for CD8α and Foxp3; bar, 80 μm. Quantifications of positive area of tumor sections with ImageJ using the geometric mean of up to 3 representative images from each tumor section, with $n = 3$–4 tumor sections for each experimental group. Error bars represent SD, *, $P < 0.05$; **, $P < 0.01$; ***, $P < 0.001$ using the two-tailed unpaired Student *t* test.

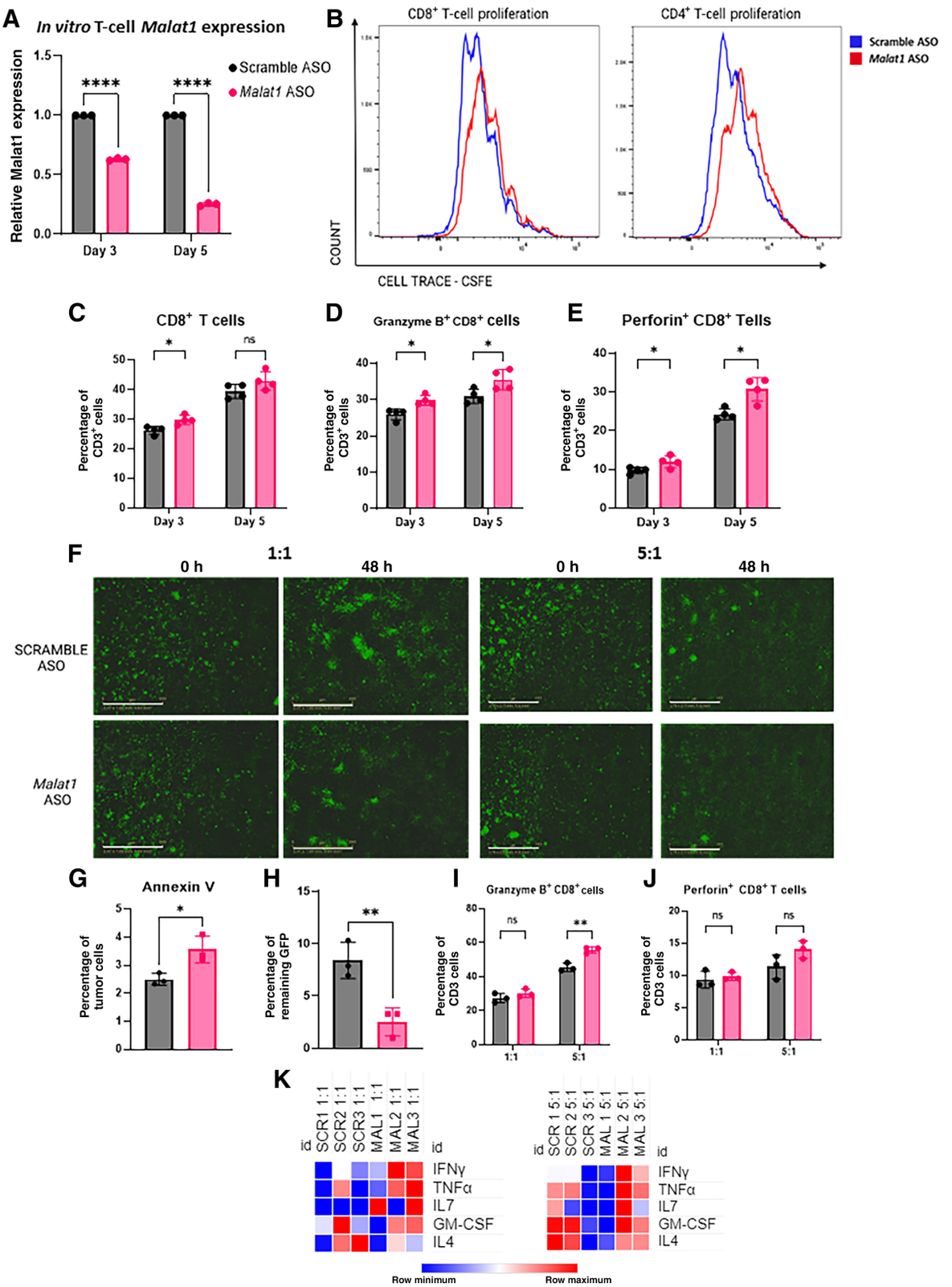
A
In vitro T-cell Malat1 expression
Relative Malat1 expression
Scramble ASO
Malat1 ASO
****
****
Day 3
Day 5
B
CD8+ T-cell proliferation
CD4+ T-cell proliferation
Scramble ASO
Malat1 ASO
COUNT
CELL TRACE - CSFE
C
CD8+ T cells
Percentage of CD3+ cells
D
Granzyme B+ CD8+ cells
E
Perforin+ CD8+ Tells
F
1:1
5:1
0 h
48 h
SCRAMBLE ASO
Malat1 ASO
G
Annexin V
Percentage of tumor cells
H
Percentage of remaining GFP
I
Granzyme B+ CD8+ cells
Percentage of CD3 cells
J
Perforin+ CD8+ T cells
K
SCR1 1:1
SCR2 1:1
SCR3 1:1
MAL1 1:1
MAL2 1:1
MAL3 1:1
SCR 1 5:1
SCR 2 5:1
SCR 3 5:1
MAL 1 5:1
MAL 2 5:1
MAL 3 5:1
IFNγ
TNFα
IL7
GM-CSF
IL4
Row minimum
Row maximum

able to prolong mouse survival (**Fig. 7D** and **E**) in these highly aggressive tumors. Of note, mice treated with single-agent ICB did not have any response as compared with the IgG control, but in combination with the *Malat1* ASO there was significant prolonged mouse survival.

Immunophenotyping the TILs isolated from the primary tumor in these treatment groups recapitulated the changes in T-cell populations seen with single-agent treatment, with an increase in cytotoxic Granzyme B^+CD8^+ T cells and a decrease in Tregs (**Fig. 7F–M**). Single-agent ICB-treated tumors had an increase in regulatory $Foxp3^+$ $CD4^+$ cells as compared with single-agent ASO or chemotherapy treatment groups, but *Malat1* ASO used in combination with ICB significantly decreased this immunosuppressive T-cell population (**Fig. 7I** and **M**). IHC staining in these treatment groups supported what was observed in the TIL flow analysis with more $CD8^+$ T cells found both inside and outside the stromal areas of the tumor in combination with *Malat1* ASO as compared with single-agent treatment (Supplementary Fig. S7A). These results highlight the potential of using *Malat1* ASO in combination with common clinically available therapies and that the immune infiltration seen in the TME may boost the efficacy of chemotherapy and ICB when used with the right staging parameters.

Discussion

This study reports the efficacy of using a systemic gapmer ASO to successfully target a lncRNA and the effects *Malat1* depletion have in two separate and quite different *in vivo* TNBC models. Previous studies have documented how *Malat1* promotes aggressive and invasive behavior in cancer cells (35, 36), and this is suggested to occur primarily through its ability to act as a ceRNA, an RNA that can compete for miRNAs and sequester miRNAs from their intended target (38, 39). With respect to breast cancer, many *in vitro* studies have shown that *Malat1* silencing decreases tumor cell proliferation, invasion, and revealed *Malat1*'s role in the epithelial-to-mesenchymal transition (21, 40–42). Arun and colleagues (22) previously have shown that treating the luminal B–like mouse model MMTV-PyMT with a *Malat1* ASO decreased the lung metastatic burden as well as increased differentiation in the primary tumor to a more cystic phenotype. Our study revealed that depletion of *Malat1* in two genetically distinct tumor models of TNBC using an ASO delays primary tumor growth, strengthening the claim that *Malat1* promotes tumor propagation in TNBC. As a single-agent treatment, the *Malat1* ASO decreased cell proliferation and increased apoptosis in tumors, but we also wanted to take advantage of these syngeneic mouse models and examine the effects *Malat1* inhibition may have in reprogramming the TME. Moreover, we wanted to determine whether creating a more immunostimulatory TME could help improve response to treatment in these aggressive preclinical models. A major roadblock to treatment efficacy is the highly immunosuppressive TME found in TNBC and many solid tumors (43, 44). Though TNBC does display an increase T-cell infiltration as compared with hormone receptor–positive breast cancers (45, 46), checkpoint markers along with other immunosuppressive factors render these T cells ineffective in complete tumor clearance. ICB has proven to be an important option in TNBC especially when used in combination with chemotherapy that creates a more immunogenic TME (47). However, chemotherapy is still necessary for an increased clinical response and even with improved immune infiltration, immunosuppressive myeloid and stromal cells are still roadblocks that hinder efficacy. In our claudin-low and luminal-like TNBC models, there is an abundance of TAMs and MDSCs, respectively, that make immunomodulatory drugs like checkpoint inhibition and chemotherapy ineffective, contributing to the acquired resistance to treatment (29). In this study, we have demonstrated in *in vivo* TNBC models that *Malat1* depletion through ASO silencing promotes an immunostimulatory TME.

The effects of *Malat1* on immune cells have been previously studied in relation to infection, cardiovascular disease, and diabetes (48–50). In certain cancers, upregulated *Malat1* expression increases angiogenesis and "M2-like" macrophage recruitment to the TME and silencing of *Malat1* helps to relieve this immunosuppression (23, 51). Single-cell analysis of neutrophils before and after direct contact with the primary tumor in PyMT-N, a neutrophil enriched mouse model, shows increased *Malat1* expression in neutrophils after coming in contact with tumor cells, revealing that part of the tumor education of neutrophils includes increasing their *Malat1* expression. These observations provide evidence that *Malat1* helps to confer the immunosuppressive capabilities of myeloid cells. We were able to determine that the depletion of *Malat1* in tumor cells intrinsically alters chemokine and cytokine secretion and diminishes the recruitment signals that tumor cells produce to increase infiltration of TAMs and MDSCs to the tumor site. The intrinsic changes to the tumor cell secretory profile may contribute to the decrease in immunosuppressive TAMs and G-MDSCs that we observed in T12 and 2208 L primary tumors, respectively. Further studies indicate that there is significant knockdown of *Malat1* RNA expression in TAMs as well $GR1^+$ MDSCs following ASO treatment, and extensive *in vitro* coculture experiments with isolated TAMs and MDSCs illustrate

Figure 6.

Malat1 inhibition in T cells increases proliferation and cell cytotoxicity. **A,** qPCR analysis of RNA extracted from T cells isolated from splenocytes from a WT BALB/c mouse cultured *in vitro* for 3–5 days in 500 nmol/L of Scramble/*Malat1* ASO display significant decrease of *Malat1* expression in the *Malat1* ASO treatment group. Relative fold change based on *Gapdh* RNA level. Experimental $n = 3$. Error bars represent standard deviation (SD). ****, $P < 0.0001$ using the two-tailed unpaired Student *t* test. **B,** Representative proliferation plot of T cells isolated from splenocytes from a WT BALB/c mouse stained with CFSE and activated with CD3/CD28 Dynabeads for 72 hours. **C–E,** Flow cytometry quantification of $CD8^+$, Granzyme B^+ and $Perforin^+$ T cells after 3 and 5 days. Data are representative of at least 2 independent experiments. Error bars represent SD. *, $P < 0.05$; **, $P < 0.01$ using the multiple Student *t* tests and the Holm–Šídák method for multiple comparisons. **F,** Representative Incucyte images of T cells isolated from the splenocytes of a WT JEDI mouse and GFP-labeled T12 tumor cell line at a 1:1 and 5:1 E:T ratio; scale bar, 800 μm. Image was taken at 0 and 48 hours. Experimental $n = 3$. **G,** Flow cytometry quantification of residual Annexin V^+ tumor cells at the 1:1 effector ratio. Error bars represent SD. *, $P < 0.05$ using the two-tailed unpaired Student *t* test. **H,** Remaining GFP signal of 5:1 T-cell:tumor cell cocultures. The percentage was calculated by dividing the total green object integrated intensity (GCU x μm^2/image) at 48 hours by the starting green object–integrated intensity (GCU × μm^2/image) × 100. GFP signal calculated using Incucyte S3. Error bars represent SD, **, $P < 0.01$ using the two-tailed unpaired Student *t* test. **I** and **J**, Flow cytometry quantification of Granzyme B^+ and $Perforin^+$ T cells after 48 hours. Error bars represent SD. *, $P < 0.05$; **, $P < 0.01$, using the multiple Student *t* tests and the Holm–Šídák method for multiple comparisons. **J,** Heat map of cytokine/chemokine array of supernatant collected from cocultures with *Malat1*-depleted Jedi T cells.

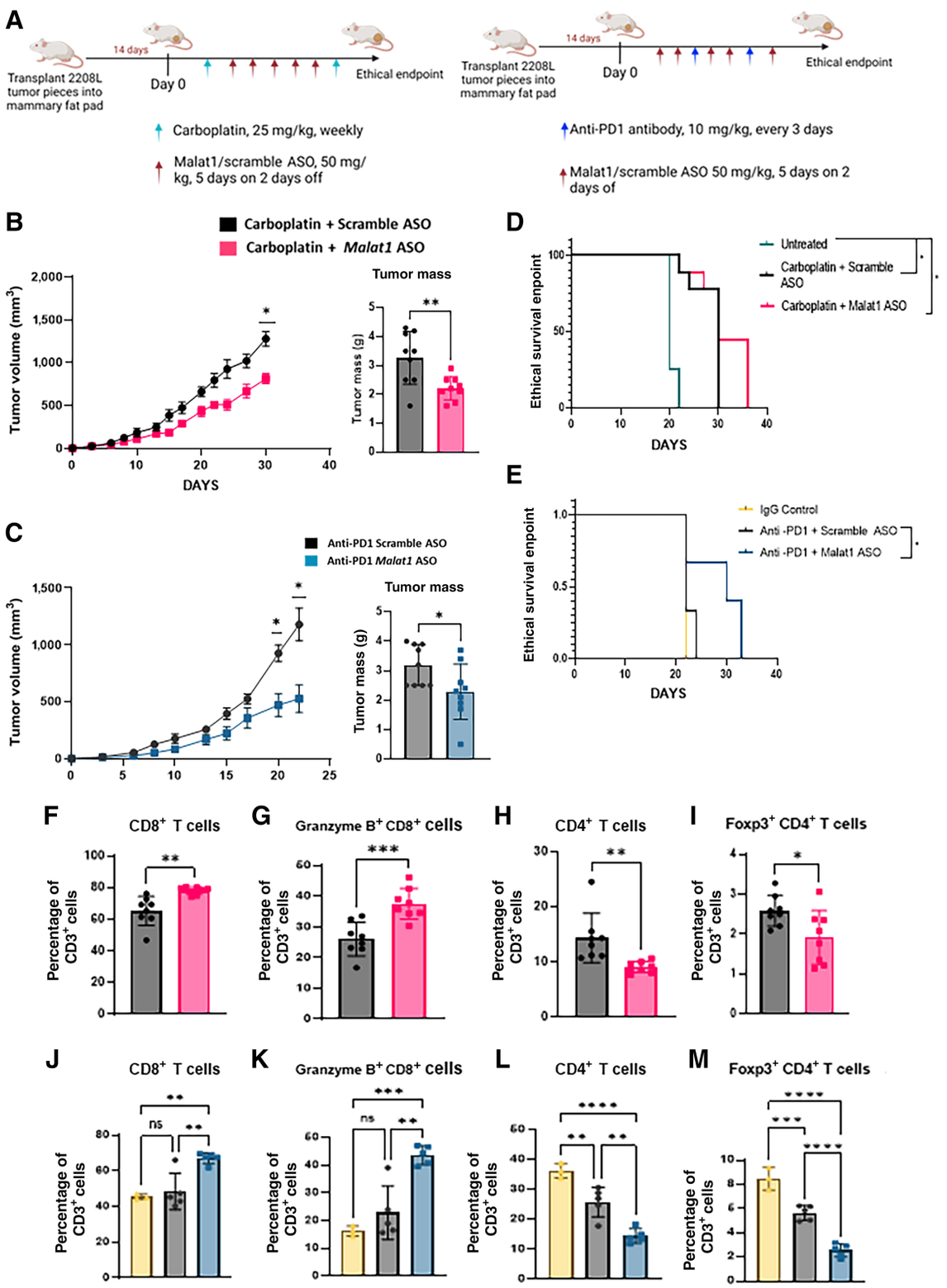
A
14 days
Transplant 2208L tumor pieces into mammary fat pad
Day 0
Ethical endpoint
Carboplatin, 25 mg/kg, weekly
Malat1/scramble ASO, 50 mg/kg, 5 days on 2 days off
Anti-PD1 antibody, 10 mg/kg, every 3 days
Malat1/scramble ASO 50 mg/kg, 5 days on 2 days of
B
Carboplatin + Scramble ASO
Carboplatin + Malat1 ASO
Tumor volume (mm3)
DAYS
Tumor mass
Tumor mass (g)
C
Anti-PD1 Scramble ASO
Anti-PD1 Malat1 ASO
D
Untreated
Carboplatin + Scramble ASO
Carboplatin + Malat1 ASO
Ethical survival enpoint
E
IgG Control
Anti -PD1 + Scramble ASO
Anti -PD1 + Malat1 ASO
F
CD8+ T cells
G
Granzyme B+ CD8+ cells
H
CD4+ T cells
I
Foxp3+ CD4+ T cells
Percentage of CD3+ cells
J
K
L
M
ns

that depleting *Malat1* in myeloid cells diminishes their immunosuppressive function. This results in increased effector function of T cells when cultured with tumor cells and *Malat1*-depleted TAMs or MDSCs. Although we observed a decrease in numerous chemokines/cytokines responsible for myeloid cell recruitment and propagation with *Malat1* knockdown in both TAMs and MDSCs, the specific decline of secreted IL10, which is known to hamper T-cell function (52, 53), may a play role in curtailing the immunosuppressive function of myeloid cells.

The effect of *Malat1* on myeloid cell populations in the TME *in vivo* led us to investigate T-cell infiltration and function within the immune landscape because the T-cell response is paramount for the efficacy of immunomodulation therapies. A recent study in COVID-19 patients found that decreased *Malat1* expression in T cells was linked to increased proliferative capabilities (54). However, there is little known about the effect *Malat1* inhibition has on T-cell infiltration and function in cancer. In this study, we discovered that when mice are treated *in vivo* with the ASO regimen, there is an increase in $CD8^+$ T-cell infiltration with a decrease in Tregs in the 2208 L model, and in both the T12 and 2208 L tumors there is increase in cytotoxic T cells. The cytokine/chemokine assays performed on tumor cells and myeloid cells did not reveal an increase in inflammatory markers that could explain the increase in infiltration and led us to look at the intrinsic effect *Malat1* depletion had on T-cell function. *Malat1* knockdown in T cells increased T-cell proliferation with an increase in cytotoxic $CD8^+$ T-cell markers Granzyme B and Perforin. In addition, *Malat1* ASO–treated GFP-targeting T cells cultured with GFP-labeled tumor cells revealed an increase in tumor cell killing with *Malat1* depletion. Unlike tumor cells and myeloid cells, there was also increased Ifnγ and Tnfα in T cell–conditioned supernatants; however we observed variability within each treatment condition that we attribute to the use of primary cells. These alterations on immune populations with *Malat1* ASO treatment suggest that the decrease in the immunosuppressive properties of tumor and myeloid cells coupled with increased cytotoxicity of T cells acts in synergy to improve the overall response observed *in vivo*.

To attribute the delay in primary tumor growth with *Malat1* ASO treatment with the changes in the TME after *Malat1* knockdown, we performed a series of treatment studies in T cell–deficient mice implanted with 2208 L tumors. In the athymic nude mouse model absent of any T cells, there was no delay in tumor growth with *Malat1* ASO treatment even with an approximate 62% reduction of *Malat1* RNA expression in the tumor, similar to the knockdown observed in BALB/c mice. Treatment of BALB/c mice with a CD8α-specific antibody along with ASO, also demonstrated no change in primary tumor growth, whereas tumors treated with the IgG control still responded to the *Malat1* ASO. These results suggest that much of the response we see with single-agent *Malat1* ASO is T-cell–mediated and may specifically be $CD8^+$ T cell–mediated. Because of the large number of myeloid cells present compared with T cells in 2208 L tissue, we believe that the changes in myeloid cell recruitment and function after *Malat1* depletion may allow for increased T-cell infiltration and cytotoxicity, contributing to the response observed.

To investigate whether changes in the TIME after *Malat1* depletion would also improve the tumor response to immunomodulatory therapies, we combined the *Malat1* ASO with anti-PD1 in the 2208 L model. The highly immunosuppressive neutrophil-enriched microenvironment in 2208 L tumors results in negligible response to checkpoint inhibition (29). In this study, combining *Malat1* ASO with anti-PD1 led to a significant decrease in primary tumor growth, tumor volume, and weight. Furthermore, we were able to significantly prolong mouse survival with this combination treatment. The effect *Malat1* depletion has on both immunosuppressive myeloid cells and T-cell infiltration may play a vital role in this improved response by promoting a more immunostimulatory microenvironment that improves checkpoint inhibition efficacy. Both IHC and flow analysis confirmed the increase in cytotoxic T-cell infiltration with combination treatment, similar to what we saw with the single-agent treatment. Of note, we also observed that ICB treatment causes an increase in regulatory $CD4^+$ T cells that is significantly reduced when combined with *Malat1* ASO. However, with the current treatment regimen we were not able to achieve tumor regression or establish PFS in these aggressive tumor models and further investigation into treatment scheduling and/or combination regimens, may provide an improved tumor response. Depleting *Malat1* expression in tumors first, followed by treatment with chemotherapy or ICB may be a promising dosing regimen and remains a possible avenue of future investigation.

In more general terms, these discoveries of the effects of *Malat1* depletion in the TNBC TME highlight the promising capabilities that targeting a lncRNA with an ASO provides. In the case of *Malat1*, which is a highly abundant lncRNA that has many possible binding partners, it was difficult to pinpoint a single effector molecule and signaling pathway responsible for the observed alterations of the immune microenvironment. Studies in the T cell–deficient mouse models point to T cells being integral to the tumor response. However, understanding whether this is due to intrinsic changes to T-cell function or the relief of immunosuppression on T cells will require

Figure 7.

Combination of *Malat1* ASO with chemotherapy or ICB improves response in preclinical mouse models. **A,** Experimental design of combination treatment studies. WT BALB/c mice had 2208 L tumor pieces implanted into the mammary fat pad and were treated with either 25 mg/kg carboplatin and ASO or 10 mg/kg anti-PD1 and ASO, once tumor was palpable (≤50 mm^3). **B,** Tumor growth curves of 2208 L tumors treated with single-agent carboplatin ($n = 9$) or in combination with *Malat1* ASO ($n = 9$) and comparison of tumor weight after harvest. *, $P < 0.05$ using mixed effects analysis to account for missing values that occurred when mouse reached ethical endpoint, with the Sidak multiple comparisons test for tumor volumes. The two-tailed unpaired Student *t* test was used for tumor weights. **C,** Tumor growth curves of 2208 L tumors treated with single-agent anti-PD1 ($n = 9$) or in combination with *Malat1* ASO ($n = 9$) and comparison of tumor weight after harvest. *, $P < 0.05$ using mixed effects analysis with the Sidak multiple comparisons test for tumor volumes and the two-tailed unpaired Student *t* test for tumor weights. **D** and **E**, Kaplan–Meier survivor curves of tumors that reach ethical endpoint (≥1,500 mm^3). *, $P < 0.05$ using a log-rank (Mantel–Cox) test. **F–I,** Flow cytometry quantification of T cells isolated from single-agent carboplatin ($n = 8$) and combination of carboplatin and *Malat1* ASO ($n = 8$) as the percentage of $CD3^+$ populations using GraphPad Prism 9.4.1. Error bars represent standard deviation (SD). *, $P < 0.05$; **, $P < 0.01$; ***, $P < 0.001$ using the two-tailed unpaired Student *t* test. **J–M,** Flow cytometry quantification of T cells isolated from IgG control ($n = 3$) single-agent anti-PD1 ($n = 5$) and combination anti-PD1 and *Malat1* ASO ($n = 5$) as the percentage of $CD3^+$ populations using GraphPad Prism 9.4.1. Error bars represent SD. *, $P < 0.05$; **, $P < 0.01$; ***, $P < 0.001$; ****, $P < 0.0001$ using one-way ANOVA and Dunnett's multiple comparisons test with an adjusted *P* value for multiple comparison.

further experimentation. We suggest that depleting *Malat1 in vivo* has led to pleiotropic effects in numerous TILs and tumor cells and these combined effects play a role in altering the immune landscape. However, single-cell sequencing of tumor cells and $CD45^+$ cells as well as proteomics will be required in future studies to provide a better understanding of the crosstalk between tumor, myeloid, and T cells occurring within the TME after *Malat1* knockdown. In this study, we chose to focus initially on the effects of *Malat1* depletion at the primary tumor site; however, understanding the effects systemic *Malat1* ASO treatment have on peripheral immune cells also should be investigated further. We provide proof of concept about the potential benefits of using an ASO therapy *in vivo* and how the effects on the TIME might improve tumor response to current therapeutics. At present, we are unaware of ongoing clinical trials targeting lncRNAs for cancer treatment as single agents or in combination with other drugs, and the primary focus of lncRNAs in cancer therapy has been on the direct effect of lncRNAs on tumor cells. Tumor progression and metastasis is a multifactorial process and the TME is an integral factor contributing to tumor growth and dissemination. The results reported in this study are only the tip of the iceberg and highlight the importance of understanding the mechanisms by which lncRNAs contribute to the TIME.

Authors' Disclosures

O. Adewunmi reports grants from National Cancer Institute (NCI) during the conduct of the study. No disclosures were reported by the other authors.

Authors' Contributions

O. Adewunmi: Data curation, formal analysis, investigation, visualization, methodology, writing–original draft, project administration, writing–review and editing. **Y. Shen:** Data curation, formal analysis, investigation, visualization, methodology, writing–original draft, project administration, writing–review and editing. **X.H.-F. Zhang:** Resources, data curation, software, methodology, writing–review and editing. **J.M. Rosen:** Conceptualization, resources, software, supervision, funding acquisition, methodology, project administration, writing–review and editing.

Acknowledgments

The research for this study was funded by NCI R01 CA16303–46 and CURES supplement grant RCA016303K. This project was also supported by the Cytometry and Cell Sorting Core at Baylor College of Medicine with funding from the CPRIT Core Facility Support Award (CPRIT-RP180672), the NIH (CA125123 and RR024574), and the assistance of Joel M. Sederstrom. Special thanks to Sergio Aguirre, Clark Hamor, Nadia Leu, and Shirley Small for helping with rodent surgery and maintenance.

The publication costs of this article were defrayed in part by the payment of publication fees. Therefore, and solely to indicate this fact, this article is hereby marked "advertisement" in accordance with 18 USC section 1734.

Note

Supplementary data for this article are available at Cancer Immunology Research Online (http://cancerimmunolres.aacrjournals.org/).

Received January 17, 2023; revised May 18, 2023; accepted August 17, 2023; published first August 21, 2023.

References

1. Bergmann JH, Spector DL. Long non-coding RNAs: modulators of nuclear structure and function. Curr Opin Cell Biol 2014;26:10–8.
2. Khalil AM, Guttman M, Huarte M, Garber M, Raj A, Rivea Morales D, et al. Many human large intergenic non-coding RNAs associate with chromatin-modifying complexes and affect gene expression. Proc Natl Acad Sci USA 2009;106:11667–72.
3. Lai F, Orom UA, Cesaroni M, Beringer M, Taatjes DJ, Blobel GA, et al. Activating RNAs associate with Mediator to enhance chromatin architecture and transcription. Nature 2013;494:497–501.
4. Li W, Notani D, Ma Q, Tanasa B, Nunez E, Chen AY, et al. Functional roles of enhancer RNAs for oestrogen-dependent transcriptional activation. Nature 2013;498:516–20.
5. Shin VY, Chen J, Cheuk IW-Y, Siu M-T, Ho C-W, Wang X, et al. Long non-coding RNA NEAT1 confers oncogenic role in triple-negative breast cancer through modulating chemoresistance and cancer stemness. Cell Death Dis 2019;10:270.
6. Fan H, Yuan J, Li X, Ma Y, Wang X, Xu B, et al. LncRNA LINC00173 enhances triple-negative breast cancer progression by suppressing miR-490–3p expression. Biomed Pharmacother 2020;125:109987.
7. Groskopf J, Aubin SM, Deras IL, Blase A, Bodrug S, Clark C, et al. APTIMA PCA3 molecular urine test: development of a method to aid in the diagnosis of prostate cancer. Clin Chem 2006;52:1089–95.
8. Hu Q, Ye Y, Chan L-C, Li Y, Liang K, Lin A, et al. Oncogenic lncRNA downregulates cancer cell antigen presentation and intrinsic tumor suppression. Nat Immunol 2019;20:835–51.
9. Heward JA, Lindsay MA. Long non-coding RNAs in the regulation of the immune response. Trends Immunol 2014;35:408–19.
10. Guo Y, Xie Y, Luo Y. The role of long non-coding RNAs in the tumor immune microenvironment. Front Immunol 2022;13:851004.
11. Dent R, Trudeau M, Pritchard KI, Hanna WM, Kahn HK, Sawka CA, et al. Triple-negative breast cancer: clinical features and patterns of recurrence. Clin Cancer Res 2007;13:4429–34.
12. National Cancer Institute Surveillance, Epidemiology, and End Results Program. [Cited 2022 Dec 10]. Available From: https://seer.cancer.gov/statistics-network/explorer/application.html.
13. Cortes J, Cescon DW, Rugo HS, Nowecki Z, Im S-A, Yusof MM, et al. Pembrolizumab plus chemotherapy versus placebo plus chemotherapy for previously untreated locally recurrent inoperable or metastatic triple-negative breast cancer (KEYNOTE-355): a randomised, placebo-controlled, double-blind, phase 3 clinical trial. Lancet 2020;396:1817–28.
14. Cortes J, Rugo HS, Cescon DW, Im S-A, Yusof MM, Gallardo C, et al. Pembrolizumab plus chemotherapy in advanced triple-negative breast cancer. N Engl J Med 2022;387:217–26.
15. Fan Y, He S. The characteristics of tumor microenvironment in triple negative breast cancer. Cancer Manag Res 2022;14:1–17.
16. Fan Y, Shen B, Tan M, Mu X, Qin Y, Zhang F, et al. TGF-β-induced upregulation of malat1 promotes bladder cancer metastasis by associating with suz12. Clin Cancer Res 2014;20:1531–41.
17. Ji Q, Zhang L, Liu X, Zhou L, Wang W, Han Z, et al. Long non-coding RNA MALAT1 promotes tumour growth and metastasis in colorectal cancer through binding to SFPQ and releasing oncogene PTBP2 from SFPQ/PTBP2 complex. Br J Cancer 2014;111:736–48.
18. Guo F, Li Y, Liu Y, Wang J, Li Y, Li G, et al. Inhibition of metastasis-associated lung adenocarcinoma transcript 1 in CaSki human cervical cancer cells suppresses cell proliferation and invasion. Acta Biochim Biophys Sin 2010;42:224–9.
19. Elbasateeny SS, Yassin MA, Mokhtar MM, Ismail AM, Ebian HF, Hussein S, et al. Prognostic implications of MALAT1 and BACH1 expression and their correlation with CTCs and Mo-MDSCs in triple negative breast cancer and surgical management options. Int J Breast Cancer 2022;2022:8096764.
20. Wang Z, Katsaros D, Biglia N, Shen Y, Fu Y, Loo LWM, et al. High expression of long non-coding RNA MALAT1 in breast cancer is associated with poor relapse-free survival. Breast Cancer Res Treat 2018;171:261–71.
21. Xiping Z, Bo C, Shifeng Y, Feijiang Y, Hongjian Y, Qihui C, et al. Roles of MALAT1 in development and migration of triple negative and Her-2–positive breast cancer. Oncotarget 2018;9:2255–67.
22. Arun G, Diermeier S, Akerman M, Chang K-C, Wilkinson JE, Hearn S, et al. Differentiation of mammary tumors and reduction in metastasis upon Malat1 lncRNA loss. Genes Dev 2016;30:34–51.
23. Hou Z-H, Xu X-W, Fu X-Y, Zhou L-D, Liu S-P, Tan D-M, et al. Long non-coding RNA MALAT1 promotes angiogenesis and immunosuppressive properties of HCC cells by sponging miR-140. Am J Physiol Cell Physiol 2020;318:C649–63.
24. Huang XJ, Xia Y, He GF, Zheng LL, Cai YP, Yin Y, et al. MALAT1 promotes angiogenesis of breast cancer. Oncol Rep 2018;40:2683–9.

25. Hong D, Kurzrock R, Kim Y, Woessner R, Younes A, Nemunaitis J, et al. AZD9150, a next-generation antisense oligonucleotide inhibitor of STAT3 with early evidence of clinical activity in lymphoma and lung cancer. Sci Transl Med 2015;7:314ra185.
26. Burel SA, Han S-R, Lee H-S, Norris DA, Lee B-S, Machemer T, et al. Preclinical evaluation of the toxicological effects of a novel constrained ethyl modified antisense compound targeting signal transducer and activator of transcription 3 in mice and cynomolgus monkeys. Nucleic Acid Ther 2013; 23:213–27.
27. Bennett CF, Swayze EE. RNA targeting therapeutics: molecular mechanisms of antisense oligonucleotides as a therapeutic platform. Annu Rev Pharmacol Toxicol 2010;50:259–93.
28. Herschkowitz JI, Zhao W, Zhang M, Usary J, Murrow G, Edwards D, et al. Comparative oncogenomics identifies breast tumors enriched in functional tumor-initiating cells. Proc Natl Acad Sci USA 2012;109: 2778–83.
29. Kim IS, Gao Y, Welte T, Wang H, Liu J, Janghorban M, et al. Immuno-subtyping of breast cancer reveals distinct myeloid cell profiles and immunotherapy resistance mechanisms. Nat Cell Biol 2019;21:1113–26.
30. Zhao N, Powell RT, Yuan X, Bae G, Roarty KP, Stossi F, et al. Morphological screening of mesenchymal mammary tumor organoids to identify drugs that reverse epithelial–mesenchymal transition. Nat Commun 2021;12:4262.
31. Zhang W, Bado IL, Hu J, Wan Y-W, Wu L, Wang H, et al. The bone microenvironment invigorates metastatic seeds for further dissemination. Cell 2021;184:2471–86.
32. Albaayit SF, Abba Y, Abdullah R, Abdullah N. Prophylactic effects of Clausena excavata Burum. f. leaf extract in ethanol-induced gastric ulcers. Drug Des Devel Ther 2016;10:1973–86.
33. Yue X, Wu W-Y, Dong M, Guo M. LncRNA MALAT1 promotes breast cancer progression and doxorubicin resistance via regulating miR-570–3p. Biomed J 2021;44:S296–304.
34. Miao Y, Fan R, Chen L, Qian H. Clinical significance of long non-coding RNA MALAT1 expression in tissue and serum of breast cancer. Ann Clin Lab Sci 2016; 46:418–24.
35. Raman D, Baugher PJ, Thu YM, Richmond A. Role of chemokines in tumor growth. Cancer Lett 2007;256:137–65.
36. Hiratsuka S, Watanabe A, Aburatani H, Maru Y. Tumour-mediated upregulation of chemoattractants and recruitment of myeloid cells predetermines lung metastasis. Nat Cell Biol 2006;8:1369–75.
37. Jiang M, Chen J, Zhang W, Zhang R, Ye Y, Liu P, et al. Interleukin-6. Front Immunol 2017;8:1840.
38. Ying L, Chen Q, Wang Y, Zhou Z, Huang Y, Qiu F, et al. Upregulated MALAT-1 contributes to bladder cancer cell migration by inducing epithelial-to-mesenchymal transition. Mol Biosyst 2012;8:2289–94.
39. Peng Y, Fang X, Yao H, Zhang Y, Shi J. MiR-146b-5p regulates the expression of long non-coding RNA. Cancer Biother Radiopharm 2021;36:433–40.
40. Xu Y, Zhang X, Hu X, Zhou W, Zhang P, Zhang J, et al. The effects of lncRNA MALAT1 on proliferation, invasion and migration in colorectal cancer through regulating SOX9. Mol Med 2018;24:52.
41. Zuo Y, Li Y, Zhou Z, Ma M, Fu K. Long non-coding RNA MALAT1 promotes proliferation and invasion via targeting miR-129–5p in triple-negative breast cancer. Biomed Pharmacother 2017;95:922–8.
42. Zhao C, Ling X, Xia Y, Yan B, Guan Q. The m6A methyltransferase METTL3 controls epithelial–mesenchymal transition, migration and invasion of breast cancer through the MALAT1/miR-26b/HMGA2 axis. Cancer Cell Int 2021; 21:441.
43. De Palma M, Lewis CE. Macrophage regulation of tumor responses to anticancer therapies. Cancer Cell 2013;23:277–86.
44. Gajewski TF, Schreiber H, Fu YX. Innate and adaptive immune cells in the tumor microenvironment. Nat Immunol 2013;14:1014–22.
45. Salgado R, Denkert C, Demaria S, Sirtaine N, Klauschen F, Pruneri G, et al. The evaluation of tumor-infiltrating lymphocytes (TILs) in breast cancer: recommendations by an international TILs working group 2014. Ann Oncol 2015;26: 259–71.
46. Denkert C, von Minckwitz G, Darb-Esfahani S, Lederer B, Heppner BI, Weber KE, et al. Tumour-infiltrating lymphocytes and prognosis in different subtypes of breast cancer: a pooled analysis of 3,771 patients treated with neoadjuvant therapy. Lancet Oncol 2018;19:40–50.
47. Schmid P, Adams S, Rugo HS, Schneeweiss A, Barrios CH, Iwata H, et al. Atezolizumab and Nab-paclitaxel in advanced triple-negative breast cancer. N Engl J Med 2018;379:2108–21.
48. Lei L, Chen J, Huang J, Lu J, Pei S, Ding S, et al. Functions and regulatory mechanisms of metastasis-associated lung adenocarcinoma transcript 1. J Cell Physiol 2018;234:134–51.
49. Gast M, Rauch BH, Nakagawa S, Haghikia A, Jasina A, Haas J, et al. Immune system-mediated atherosclerosis caused by deficiency of long non-coding RNA MALAT1 in ApoE$^{-/-}$ mice. Cardiovasc Res 2019;115:302–14.
50. Hewitson JP, West KA, James KR, Rani GF, Dey N, Romano A, et al. Suppresses immunity to infection through promoting expression of Maf and IL10 in Th cells. J Immunol 2020;204:2949–60.
51. Huang J-K, Ma L, Song W-H, Lu B-Y, Huang Y-B, Dong H-M, et al. LncRNA–MALAT1 promotes angiogenesis of thyroid cancer by modulating tumor-associated macrophage FGF2 protein secretion. J Cell Biochem 2017;118: 4821–30.
52. Moore KW, de Waal Malefyt R, Coffman RL, O'Garra A. Interleukin-10 and the interleukin-10 receptor. Annu Rev Immunol 2001;19:683–765.
53. Smith LK, Boukhaled GM, Condotta SA, Mazouz S, Guthmiller JJ, Vijay R, et al. Interleukin-10 directly inhibits CD8. Immunity 2018;48:299–312.
54. Dey S, Ashwin H, Milross L, Hunter B, Majo J, Filby AJ, et al. Downregulation of MALAT1 is a hallmark of tissue and peripheral proliferative T cells in COVID-19. Clin Exp Immunol 2023;212:262–75.